HHS Public Access

Author manuscript

Dev Cell. Author manuscript; available in PMC 2020 March 25.

Published in final edited form as:

Dev Cell. 2019 March 25; 48(6): 765–779.e7. doi:10.1016/j.devcel.2019.01.017.

YAP Partially Reprograms Chromatin Accessibility to Directly Induce Adult Cardiogenesis *in Vivo*

Tanner O. Monroe[1], **Matthew C. Hill**[3], **Yuka Morikawa**[2], **John P. Leach**[1,#], **Todd Heallen**[2], **Shuyi Cao**[1,4], **Peter H. L. Krijger**[5], **Wouter de Laat**[5], **Xander H.T. Wehrens**[1,4], **George G. Rodney**[1,4], and **James F. Martin**[1,2,3,4,*]

[1]Department of Molecular Physiology and Biophysics, Baylor College of Medicine, One Baylor Plaza, Houston, Texas, 77030. [2]Cardiomyocyte Renewal Lab, Texas Heart Institute, 6770 Bertner Avenue, Houston, Texas, 77030. [3]Program in Developmental Biology, Baylor College of Medicine, One Baylor Plaza, Houston, Texas, 77030. [4]Cardiovascular Research Institute, Baylor College of Medicine, One Baylor Plaza, Houston, Texas, 77030. [5]Oncode Institute, Hubrecht Institute-KNAW and University Medical Center Utrecht, Utrecht, the Netherlands.

Summary:

Specialized adult somatic cells, such as cardiomyocytes (CMs), are highly differentiated with poor renewal capacity, an integral reason underlying organ failure in disease and aging. Among the least renewable cells in the human body, CMs renew approximately 1% annually. Consistent with poor CM turnover, heart failure is the leading cause of death. Here, we show that an active version of the Hippo pathway effector YAP, termed YAP5SA, partially reprograms adult mouse CMs to a more fetal and proliferative state. One week after induction, 19% of CMs that enter S-phase do so twice, CM number increases by 40%, and YAP5SA lineage CMs couple to pre-existing CMs. Genomic studies showed that YAP5SA increases chromatin accessibility and expression of fetal genes, partially reprogramming long-lived somatic cells *in vivo* to a primitive, fetal-like, and proliferative state.

Graphical Abstract

[*]Corresponding author and Lead Contact: Dr. James F. Martin, Department of Molecular Physiology and Biophysics, Baylor College of Medicine, and Cardiomyocyte Renewal Laboratory, Texas Heart Institute, One Baylor Plaza, Houston, Texas, 77030; Tel: 713-798-5931; jfmartin@bcm.edu.

[#]Current address: Department of Medicine, Penn Center for Pulmonary Biology, Penn Cardiovascular Institute, Penn Institute for Regenerative Medicine, University of Pennsylvania, Philadelphia, PA 19104, USA.

Author Contributions

Conceptualization: T.O.M., J.P.L., J.F.M. Formal Analysis: T.O.M., M.C.H., P.H.L.K., Investigation: T.O.M., M.C.H., J.P.L, Y.M., T.H., P.H.L.K., S.C. Resources: W.d.L. G.G.R., X.H.T.W., J.F.M. Writing – Original draft: T.O.M. Writing – Reviewing & Editing: T.O.M., J.P.L, M.C.H., J.F.M. Visualization: T.O.M. Supervision: J.F.M. Funding Acquisition: W.d.L., G.G.R, X.H.T.W., J.F.M.

Declaration of Interests

J.P.L and J.F.M. report patent US9732345B2 for Hippo pathway inhibitor.

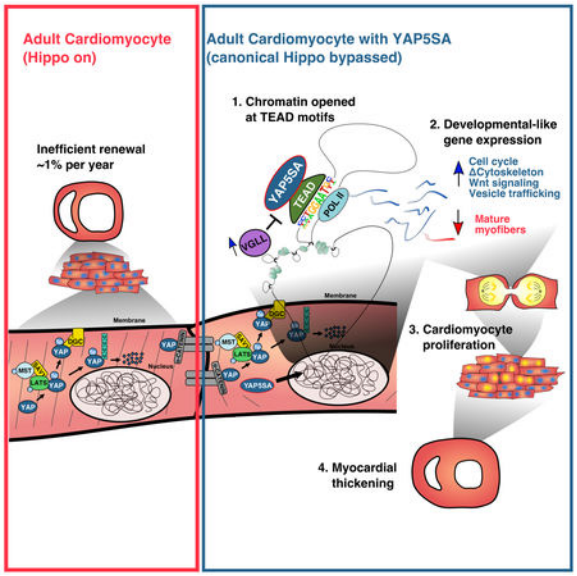

In Brief (eTOC)

As highly differentiated cells, cardiomyocytes have poor renewal capacity, a contributing factor to heart failure in aging and disease. Monroe et al. created a mouse conditionally overexpressing active YAP (YAP5SA) and show that YAP5SA expression induces adult cardiomyocytes to adopt a more proliferative state with fetal-like chromatin and transcriptional landscapes.

Introduction

Organs such as heart and brain contain long-lived, poorly renewable parenchymal cells such as cardiac myocytes (CMs) and most neurons (Bergmann et al., 2015; Frisen, 2016; Sorrells et al., 2018). Carbon-14 dating experiments revealed that a complete supply of human CMs is established within the first month of life, and adult human CMs renew at a rate of approximately 1% per year (Bergmann et al., 2015). In adult mice, CMs have similarly low rates of renewal (Alkass et al., 2015; Soonpaa and Field, 1997).

Many long-lived cells are highly specialized, such as CMs and neurons, and express cell-type specific proteins essential for function. CMs have a structured contractile apparatus, called the sarcomere that is essential for contractility. It is thought that the sarcomere poses a physical barrier that prevents CM cytokinesis (Tzahor and Poss, 2017). The metabolic state of CMs, which utilize oxidative phosphorylation, also contributes to poor renewal (Puente et al., 2014). Another barrier to CM renewal likely occurs at the epigenetic level. During development, the fate of differentiated cells is determined by the gradual restriction of the chromatin landscape from the embryonic state to that of lineage-restricted and differentiated cell (Nord et al., 2013; Stergachis et al., 2013). The chromatin state of a differentiated CM is considered to be stable and irreversible. Reversion to a more developmental cell state, as defined by chromatin accessibility, has been described in cancer but not in tissue renewal (Denny et al., 2016; Stergachis et al., 2013; Zhu et al., 2013).

The long-lived and specialized nature of CMs led to the notion that improving endogenous CM renewal was an ineffectual strategy to treat heart disease. Recent work revealed that CMs can be induced to renew by expressing exogenous factors, such as cell cycle components or microRNAs (Mohamed et al., 2018; Wang and Martin, 2014; Xin et al., 2013), and through physiologic means such as exercise (Vujic et al., 2018). To develop effective therapies, it is important to uncover intrinsic molecular mechanisms that inhibit CM renewal (Tzahor and Poss, 2017).

The Hippo pathway, a kinase cascade, suppresses transcriptional activity of YAP by phosphorylating Serine (S) residues at five NDR (nuclear Dbf2-related) kinase family motifs, (HXRXXS)(Halder and Johnson, 2011) *via* large tumor suppressor (Lats)1 and Lats2. Deletion of upstream Hippo pathway genes or expressing an active YAP with a single serine (S) to alanine (A) mutation results in increased CM renewal (Heallen et al., 2013; Lin et al., 2014; Morikawa et al., 2015; Xin et al., 2013). Recent work revealed that the Hippo pathway was upregulated in human heart failure (HF) and Hippo pathway deficiency in mice reversed systolic HF, supporting the notion that the Hippo pathway is an endogenous genetic pathway that can be manipulated to improve CM renewal (Leach et al., 2017). Previous experiments inactivating Hippo pathway components left considerable residual CM Hippo activity. We hypothesized that more completely bypassing Hippo pathway negative regulation would more efficiently increase adult CM renewal and afford us the opportunity to study YAP activity in greater depth. To circumvent the physiologic inputs that activate Hippo and inhibit YAP, we generated mice that conditionally overexpress YAP5SA, a version of YAP that has all LATS1/2 phosphorylation sites mutated from S to A, in adult CMs (Zhao et al., 2010). YAP5SA globally reprograms adult CM chromatin accessibility at select genomic regions to promote a more renewable state.

Results

Generation of a YAP5SA gain-of-function transgenic mouse

We made a Cre-inducible YAP5SA transgene containing a LoxP-flanked eGFP-STOP cassette, a Flag-tagged YAP5SA and IRES LacZ reporter for lineage tracing that directed eGFP expression in embryonic and postnatal hearts before Cre recombination (Fig. 1A-E). We crossed YAP5SA mice to tamoxifen (tam)-inducible, cardiomyocyte-specific Cre driver, αMyHC-Cre-ERT2 (MCM) to generate mice with YAP5SA overexpressing (OE) CMs (Sohal et al., 2001). To activate YAP5SA in adult CMs, we performed daily tam injections (40μg/g) for four consecutive days in a “high dose” injection regimen. Western blots showed a 5-fold increase in YAP levels in YAP5SA OE hearts compared to controls (Fig. 1F,G) one day after the fourth tam injection. We noted an increase in endogenous P-YAP levels that we discuss below (Fig. 1F,H). Yap immunofluorescence (IF) revealed increased nuclear and cytoplasmic YAP with varying intensities suggesting that not all Yap5SA expressing CMs had constitutive nuclear Yap activity (Fig. 1I,J). Since CMs expressing low levels of nuclear Yap may be non-transgenic CMs, we performed Flag IF to look at Yap5SA CM expression. In Yap5SA CMs, nuclear Flag expression also varied over a wide range and was increased on average approximately 3.2 fold over cytoplasmic Flag (Fig. 1K). We conclude that the Yap5SA OE mice had an increase in nuclear and cytoplasmic Yap in adult CMs but that

Yap5SA subcellular localization was still regulated through Hippo-independent mechanisms such as interaction with the intercalated disc (ICD) as we found previously (Morikawa et al., 2017).

YAP5SA hearts have thickened ventricular walls and smaller chambers

One day after the fourth tam injection, echocardiography (ECHO) showed thickened ventricular walls, decreased chamber size, and increased ejection fraction in YAP5SA OE hearts compared to the same mice pre-tam and tam-injected MCM controls (Fig. 1L, Fig. S1A; Supplemental videos 1-2). Compared to before tam, YAP5SA OE hearts increased ejection fraction (59.1 +/− 3.5% to 72.5 +/− 4.7%) and fractional shortening (30.9 +/− 1.4% to 41.4 +/− 3.5%) while the left ventricular (LV) chamber diameters decreased from 2.66 +/− 0.15 to 1.87 +/− 0.28 mm in systole (ESD) and 3.84 +/− 0.17 to 3.14 +/− 0.25 mm in diastole (EDD), resulting in decreased cardiac output. YAP5SA OE hearts had increased posterior free wall width in systole (FWWS) from 1.05 +/− 0.03 to 1.38 +/− 0.06 mm and in diastole (FWWD) from 0.78 +/− 0.03 to 1.01 +/− 0.04 mm (Fig. S1A). Two days after the final tam injection, the LV chambers were reduced (Fig. 1M). Histology of YAP5SA OE hearts three days after the fourth tam injection also revealed an increased LV wall thickness and smaller chamber (Fig. 1N).

YAP5SA OE mice died within four days after the last tam dose as a result of HF. Necropsy showed that YAP5SA OE mice had signs of HF including pleural effusion, ascites, interstitial pulmonary edema (Fig. S1B). Controls, which included MCM/YAP5SA treated with oil and MCM treated with tam, did not exhibit HF (Fig. 1O). There was no difference in CM size, number, or heart size between MCM/YAP5SA and MCM mice before tam administration (Fig. S1 C-E).

YAP5SA cardiomyocytes progress through the cell cycle

To quantify S-phase entry in adult YAP5SA OE CMs, we provided nucleotide analog, EdU (5-ethynyl-2'-deoxyuridine) *ad-libitum* in drinking water for two days following high dose tam regimen. EdU incorporation was undetectable in control MCM and MCM/YAP5SA CMs without tam consistent with previous data (Fig. 2A,B) (Alkass et al., 2015; Soonpaa and Field, 1997). Approximately 16% of YAP5SA OE CMs were EdU positive (Fig. 2A,B). We also administered EdU for the entire four day tam protocol and performed Flag IF experiments to visualize YAP5SA. Two days after the last tam injection, for a total of six EdU days, 40% of CMs expressed nuclear YAP5SA as determined by Flag IF. Of the nuclear Flag positive CMs, 10% were also EdU-positive. Interestingly, 20% of CMs that were negative for nuclear Flag were EdU-positive (Fig. S1F,G) indicating a population of YAP5SA OE CMs that had entered S-Phase and extinguished nuclear YAP5SA. Alternatively, there may be a paracrine effect of YAP5SA OE CMs on neighboring CMs that do not express YAP5SA.

We investigated mitotic marker expression two days after the fourth tam dose. Phosphorylation of Histone H3-Ser10 (pHH3) by Aurora Kinase B (AURKB) occurs during chromosome condensation (prophase) and persists throughout metaphase before a decline at anaphase and later stages of mitosis. In contrast, the chromosomal passenger protein

AURKB is detected more broadly throughout M-phase and cytokinesis (Sawicka and Seiser, 2012). Approximately 1% of YAP5SA OE CMs were pHH3-positive (Fig. 2C-D), and 11% nuclear AURKB-positive (Fig. 2E,F), providing support that YAP5SA OE CMs were proliferative. While most AURKB expression was nuclear, we found AURKB in dividing CMs in the cytokinesis remnant, albeit it more rarely (Fig. 2 E-G).

To test whether YAP5SA CMs progressed through the cell cycle multiple times, we performed a double labeling experiment using a single low dose tam injection to induce YAP5SA in a low number of CMs (STAR Methods). After single tam injection, mice were pulsed with EdU for three days, with a two-day washout, followed by another three-day BrdU (5-Bromo-2'-deoxyuridine) pulse (Fig. 2H). To identify CM nuclei, we used WGA (Fig. 2I), Pericentriolar material 1 (PCM-1) (Fig. S1H), or cTnT (Fig. S1I). We detected 4.25% EdU-labeled and 5.04% BrdU-labeled CM nuclei, indicating comparable labeling for both analogs (Fig. 2H-J, Fig. S1H,I). Of EdU-labeled CM nuclei, approximately 19% were also BrdU positive (0.83% total double positive) (Fig. 2J). These findings support the conclusion that proliferative YAP5SA OE CMs are capable of cycling more than once.

YAP5SA hearts have cardiomyocyte hyperplasia

To estimate CM number in LV, we used stereology on hearts harvested two days after the fourth tam injection of the high dose regimen. Hearts were sectioned from apex to base in 7-μm increments and LV area measured at different tissue depths. LV volume was calculated by plotting LV area as a function of location and integrating the area under the curve. Compared to controls, YAP5SA OE hearts had increased LV muscle volume, and decreased chamber volume (Fig. 2K-M, Fig. 1M). YAP5SA OE hearts had an increased ratio of LV weight to body weight, but CMs were smaller (Fig. 2N,O). Controls were MCM mice (with and without) tam and MCM/YAP5SA mice without tam.

To estimate LV CM number, we calculated the density of PCM-1-positive CM nuclei in control and YAP5SA OE hearts (73,000 +/− 3000 CM nuclei/mm^3 vs 70,600 +/− 1300 CM nuclei/mm^3 respectively) (Alkass et al., 2015; Bergmann et al., 2015). Our CM nuclei density data were consistent with mouse stereology data previously reported (Alkass et al., 2015). We multiplied CM density by total heart volume and corrected for CM nucleation (see below) (Alkass et al., 2015; Bergmann et al., 2015). Compared to controls, YAP5SA OE hearts had a large increase in the number of LV CMs (1,840,000 +/− 39,000 vs. YAP5SA: 2,680,000 +/− 54,000 respectively; Fig. 2P,Q). Our control CM number data were consistent with previously published mouse data (Bersell et al., 2009). Controls were MCM mice with and without tam and MCM/YAP5SA mice without tam. Our data suggest that YAP5SA induces the genesis of new CMs.

Mononuclear diploid cardiomyocytes are enriched in YAP5SA hearts

We next examined nucleation and ploidy in YAP5SA CMs. It was reported that an increase in mononuclear CMs improved renewal capacity, while an increase in ploidy was deleterious for CM renewal in mice and zebrafish (Gonzalez-Rosa et al., 2018; Kadow and Martin, 2018; Patterson et al., 2017). In isolated CMs two days after the fourth tam injection, we found an increased proportion of mononuclear CMs in YAP5SA OE hearts but no change in

bi-nucleated CMs compared to tam-injected MCM controls. YAP5SA OE hearts also had a reduced proportion of CMs with 4 nuclei (Fig. S1J).

To determine DNA content of EdU-containing nuclei in YAP5SA CMs, we used the high dose tam regimen and injected EdU along with the third and fourth tam injections. Quantification of nuclear DNA content by flow cytometry 24 hours after the last tam injection revealed that in EdU-positive CM nuclei from YAP5SA OE hearts, approximately 28% of CM nuclei were diploid and 35% tetraploid, revealing that at least 28% of EdU-labeled nuclei divided. A further 35% were in S-phase, most likely intermediate between the diploid and tetraploid states (Fig. S1K-M). In total CM nuclei, we saw an increase in 2-4N and 4N nuclei but no increase in greater than 4N nuclei compared to tam-injected MCM controls (Fig. S1N). These data, along with our double labeling experiments, reveal productive YAP5SA OE CM proliferation with more mononuclear CMs without evidence of increased CM ploidy.

YAP5SA OE lineage cardiomyocytes couple with pre-existing cardiomyocytes

Because YAP5SA OE mice died after high dose tam injection regimen (Fig. 1O), we investigated whether YAP5SA mice had arrhythmias. Optical mapping 48 hours after high dose tam regimen indicated a continuous spread of action potential across the surface myocardium in YAP5SA OE hearts with a mildly reduced conduction velocity in YAP5SA OE LVs, resulting from the thickened ventricular wall, but no evidence of ventricular arrhythmias (Fig. S2A,B, Supplementary video 3). Telemetry electrocardiogram recordings similarly indicated that YAP5SA OE mice did not have severe arrhythmias, even when challenged with tam that causes T-wave inversion, as a consequence of transient Cre or tam toxicity in CMs 24 hours after tam (Bersell et al., 2013; Pugach et al., 2015) (Fig. S2 C,D). We observed clusters of lineage-traced β-gal positive YAP5SA OE CMs and 94% of these β-gal positive CMs were coupled to surrounding CMs at ICDs, as indicated by N-cadherin IF (Fig. S2E). Of β-gal positive CMs that coupled to other CMs, 37% coupled only to other YAP5SA OE lineage β-gal positive CMs, 22% coupled to β-gal negative CMs only, and 41% coupled to both β-gal positive and β-gal negative CMs (Fig. S2F).

To measure YAP5SA OE CM contractility, we isolated CMs 24 hours after the final tam injection of high dose regimen and measured individual CM contractility. Compared to tam-injected MCM controls, YAP5SA OE CMs had similar resting sarcomere length and contractility in response to field stimulation (Fig. S2G-I). YAP5SA induction did not induce interstitial fibrosis although we noted that there was a 20% increase in number and space occupied by non-CMs, compared to tam-injected MCM controls (Fig. S2J-M). The total volume of non-CMs increased as the hearts grew (0.33×10^{10} μm^3 to 0.55×10^{10} μm^3), but the increase of non-CM volume only accounted for approximately 12% of the total myocardium volume difference between MCM control to YAP5SA OE hearts (Con: 5.38×10^{10} μm^3; YAP5SA: 7.22×10^{10} μm^3) (Fig. 2M, Fig. S2L).

YAP5SA cardiomyocytes acquire a more primitive cell state

We performed CM-specific nuclear RNA-sequencing, Assay for Transpose Accessible Chromatin (ATAC)-sequencing, and chromatin conformation capture assays (3C and 4C)

two days after the fourth tam injection of the high dose regimen (Buenrostro et al., 2013; Gilsbach et al., 2014; Preissl et al., 2015) (Fig. 3A). In YAP5SA OE CMs, nuclear RNA-seq indicated that 734 genes were up-regulated whereas 282 were down-regulated compared to control, tam-injected MCM mice (adjusted p-value < 0.01) (Fig. 3B, Fig. S3A). Gene ontology and gene set enrichment analysis using existing data revealed that gene expression changes in YAP5SA OE CMs were consistent with a more primitive, proliferative CM phenotype (Fig. 3C-D, Fig. S3B) (Uosaki et al., 2015). Upregulated cell cycle genes included centromere genes; *Incenp, Cenpe* and *Cenpf;* cyclins *Ccndl, Ccna2, Ccnb2, Ccnbl;* and pro-proliferative transcription factors, *E2f2, E2f1,* and *Myc.* Another upregulated gene was *Dock2,* encoding a Rho family guanine nucleotide exchange factor, which promotes cytoskeletal remodeling and cell proliferation (Guo and Chen, 2016)(Fig. 3C). Downregulated genes included genes characteristic of adult CMs, such as genes encoding sarcomeric proteins MYH6 and TNNT1 and ion channel RYR2 (Fig. 3C).

Hippo pathway genes were increased in YAP5SA OE CMs, revealing a negative feedback loop that has been observed in other contexts (Dai et al., 2015; Moroishi et al., 2015; Park et al., 2016). The Hippo pathway genes *Lats2, Mst1 (Stk4)* and *Kibra (Wwc1)* were upregulated, as were genes encoding YAP inhibitors CRB2, AMOT, and VGLL2–4 (Fig. 3C), consistent with Western blots revealing increased YAP serine 112 (mouse analog of human serine 127) phosphorylation, an indication of increased Hippo activity (Fig. 1F,H). Together, our gene expression data revealed that YAP5SA OE CMs, although still capable of contracting and coupling to neighboring CMs, adopted a less mature cell state.

YAP5SA increases chromatin accessibility at TEAD elements

Chromatin accessibility changes are known to occur during development and in cancer, but not in adult tissue renewal (Denny et al., 2016; Stergachis et al., 2013; Zhu et al., 2013). By quantifying chromatin accessibility using ATAC-seq, we revealed reorganization of chromatin accessibility in YAP5SA OE CMs compared to MCM control, with 16,189 newly accessible ATAC-seq peaks and 13,353 less accessible ATAC-seq peaks (P < 0.035) (Fig. 4A, Fig. S3C). Unbiased motif discovery within newly accessible ATAC-seq peaks showed that the top three enriched motifs in YAP5SA OE CMs were TEAD family transcription factors (Fig. 4B). TEAD is required for YAP-dependent transcription, as YAP does not bind DNA directly (Halder and Johnson, 2011). Other enriched motifs in newly accessible peaks were AP-1 elements, which is consistent with previous YAP ChIP-seq data (Kalfon et al., 2017; Stein et al., 2015; Zanconato et al., 2015) (Fig. 4B). In genomic loci with reduced accessibility in YAP5SA OE CMs, we detected enrichment for AP-1 and myocyte enhancer factor 2A (MEF2A) motifs, suggesting that the CM differentiation program was attenuated in YAP5SA OE CMs, since MEF2A maintains CM differentiation (Naya et al., 2002) (Fig. 4B). Heat maps, displaying data for all control and YAP5SA OE CM ATAC-seq peaks, illustrated many newly accessible TEAD motifs throughout the genome in YAP5SA CMs and different accessibility of AP-1 motifs in YAP5SA CMs compared to MCM controls (Fig. 4C).

We filtered for unique ATAC-seq peaks in control and YAP5SA OE CM and performed motif analysis (Fig. S3D). TEAD, AP-1, and MEF2A motif density plots, centered on

control or YAP5SA OE unique ATAC-seq peaks, showed strong enrichment for TEAD elements in YAP5SA OE peaks. Relative to YAP5SA OE, control unique ATAC-seq peaks had an absence of TEAD elements as shown by the flat graph in Fig S3D. AP-1 elements were found in both control and YAP5SA OE peaks while MEF2A motifs were enriched only in unique control peaks (Fig. S3D). To investigate nucleosome occupancy at TEAD motifs, we used the Nucleo-ATAC algorithm and found that TEAD sites were globally depleted of nucleosomes in YAP5SA OE CMs (Schep et al., 2015) (Fig. 4D). These data are consistent with YAP5SA increasing chromatin accessibility at TEAD motifs while concurrently reorganizing AP-1 accessibility genome-wide.

YAP5SA increases accessibility of developmental cardiac enhancers in the adult

We plotted intergenic ATAC-seq peaks relative to the nearest transcription start sites (TSSs) and found a bimodal distribution of promoter-containing regions (<1kb from TSS) and distal loci (>10kb) in both control and YAP5SA OE CMs (Fig. 4E). ATAC-seq peaks unique to either MCM control or YAP5SA OE CMs (adjusted p-value < 0.01) were located in distal enhancer regions (Fig. 4E). YAP has been shown to act primarily at enhancers (Buenrostro et al., 2013; Zanconato et al., 2015) and it has been shown that YAP-TEAD binding sites are enriched for H3K27Ac, a marker of active chromatin (Morikawa et al., 2015). Comparison of our ATAC-seq data to existing H3K27Ac ChIP-seq data from E14.5 embryonic and P56 adult hearts revealed that ATAC-seq peaks unique to YAP5SA OE CMs (adjusted P-value < 0.01) were enriched for E14.5 embryonic H3K27Ac chromatin marks, indicating YAP5SA OE CMs utilize embryonic cardiac enhancers. Conversely, ATAC-seq peaks unique to control CMs (adjusted P-value < 0.01) showed enrichment for adult H3K27Ac chromatin marks (Nord et al., 2013) (Fig. 4F).

We compared our RNA-seq and ATAC-seq data to available RNA-seq (GSE112055) and H3K27Ac ChIP-seq data (GSM2497652 & GSM2687477 in GSE95143) from mouse HF samples (Kokkonen-Simon et al., 2018; Nomura et al., 2018). In the RNA-seq data, there was no correlation between differentially expressed genes from YAP5SA OE CMs and HF samples (Fig. S4A). Comparison of our ATAC-seq to the HF enhancers revealed no enrichment of HF enhancers in Yap5SA OE accessible chromatin (Fig. S4B,C). The top motifs enriched in HF enhancers include MEF2 motifs that are decommissioned rather than enriched in YAP5SA OE ATAC-seq data (Fig. S4D, Fig. 4B). Together these data indicate that in adult CMs, YAP5SA increases chromatin accessibility at developmental cardiac enhancers and this change in chromatin accessibility is distinct from that observed in HF.

Categories of YAP5SA target genes in adult cardiomyocytes

To identify direct YAP target genes, we integrated our RNA-seq and ATAC-seq datasets with available YAP ChIP-Seq data (Croci et al., 2017). Similar to our ATAC-seq data, motif analysis of YAP ChIP-seq peaks showed enrichment for TEAD and AP1 motifs (Fig. 5A,B). Centering our ATAC-seq data around YAP ChIP-seq peaks revealed that many YAP target genes are already accessible, while others are made newly accessible by YAP5SA. We categorized transcriptionally activated YAP5SA targets into: 1) genes that were already accessible, without a difference in ATAC-seq peaks between control and YAP5SA OE CMs; and 2) genes that were made newly accessible by YAP5SA. We found 293 genes that were

transcriptionally up-regulated ($P < 0.01$) with YAP ChIP-Seq peaks at accessible TEAD motifs. Of those direct YAP5SA targets, 88 loci had increased chromatin accessibility, whereas the other 205 YAP5SA targets were already accessible in YAP5SA OE CMs (ATAC-seq adjusted p-value $< 10^{-5}$) (Fig. 5C-F, Table S1).

We also looked more closely at the TEAD/AP-1 driven gene program. We subcategorized newly accessible YAP5SA targets genes that had both TEAD and AP-1 motifs and found that 85% of newly opened YAP5SA target genes with TEAD motifs also contained AP-1 motifs. These genes included several WNT signaling regulators and genes associated with developmental morphogenesis, consistent with our data that YAP5SA activates a primitive, fetal-like gene program in adult CMs (Fig. 5C,G Table S1).

Cell cycle genes: YAP5SA directly up-regulated genes encoding proteins that regulate all cell cycle phases. Many YAP5SA-regulated cell cycle genes were already accessible (RNA up; ATAC-seq no change; TEAD motif accessible YAP ChIP-seq target). These include genes that promote the transition through G2/M and G1/S, such as *Ccndl* and *Dbf4,* as well as mitosis-associated genes *Mki67,* and *Anln* (Fig. 5E, Table S1, Fig. S5). Genes involved in asymmetric cell division, such as *Prkci,* required for directed CM proliferation during trabeculation, and *Numbl,* which orients mitotic spindle and is required for proper myocardial trabeculation, were direct targets with already accessible chromatin (Passer et al., 2016; Zhao et al., 2014) (Fig. 5E, Table S1). *Insc,* responsible for spindle orientation in asymmetric cell division, was a newly accessible YAP5SA target (Kraut et al.) (Fig. 5F, Table S1, Fig. S5).

Adherens junction (AJ) assembly and cytoskeletal genes: Among the 88 genes that were made newly accessible by YAP5SA (RNA-seq up; ATAC-seq up, YAP ChIP in open TEAD motifs) were genes that promote AJ assembly, such as *Ajuba, Amotl2, Mtss1,* and *Ctnnd2,* providing insight into how new CMs functionally integrate into the heart (Fig. 5F, Table S1, Fig. S5)(Saarikangas et al., 2011). Genes encoding proteins that regulate the actin cytoskeleton were also newly accessible YAP5SA targets (Morikawa et al., 2015). *Pak3* encodes a protein that regulates actin cytoskeleton by modulating small GTPase activity (Felix et al., 2015; Hiramoto-Yamaki et al., 2010) whereas *Cobl and Fmn1* encode actin nucleators (Hou et al., 2015; Li et al., 2015b)(Fig. 5F, Table S1, Fig. S5).

Signaling pathways: Hippo pathway components were direct YAP5SA targets indicating that YAP5SA directly activates a negative feedback loop to prevent CM proliferation (Fig. 1F & H, Fig. 5F, Table S1, Fig. S5). Hippo pathway genes that are direct YAP5SA targets with newly accessible chromatin included *Lats2, Vgll2, Vgll3, Vgll4,* and *Wwc1* (Halder and Johnson, 2011) (Fig. 5F, Table S1, Fig. S5). Multiple WNT components were upregulated direct targets, including *Dab2,* which encodes an endocytic adaptor protein that functions as a WNT inhibitor, as well as *Wls*, which is essential for endosomal trafficking of WNT ligands (Hausmann et al., 2007; Hofsteen et al., 2016). Additionally, *Fzd5, Wispl, Zeb2* were also direct targets, with *Zeb2* and *Wls* being newly accessible (Fig. 5G, Table S1, Fig. S5). WNT signaling controls many aspects of cardiac development, a process associated with many newly accessible direct YAP5SA targets. Other cardiac development genes

include *Noggin,* and *Cited2* (Fig. 5F,G, Table S1, Fig. S5). Up-regulation of developmental pathways supports our model that YAP5SA promotes a fetal-like state in adult CMs.

To more fully validate YAP target genes, we assayed chromatin topology of YAP target genes in YAP5SA CMs. Based on our ATAC-seq and RNA-seq data, we selected *Nog* and *Wls* for topological analysis. 4C chromosome conformation capture (4C-seq), a method that generates detailed and unbiased chromatin contact profiles, with the *Nog* and *Wls* promoters as viewpoints revealed that ATAC-seq peaks at distal regulatory elements made contact with both the *Nog* and *Wls* promoters in YAP5SA CMs supporting our hypothesis that *Nog* and *Wls* are direct YAP targets (Fig. 5F,G). We assayed several YAP5SA target loci using targeted chromatin conformation capture (3C) (Fig. 6A,B). Consistent with our 4C-seq data, both *Nog* and *Wls* promoters displayed significant topological contacts in YAP5SA CMs (Fig. 6A). For every enhancer-promoter pair investigated across six loci, YAP5SA OE had increased enhancer-promoter contacts compared to MCM controls (see STAR methods) (Fig. 6A-C). These data are consistent with the hypothesis that YAP5SA OE causes local chromatin conformational changes that loop accessible TEAD motif-containing regulatory elements into contact with their promoters to increase gene expression.

Discussion

Manipulating long-lived specialized cells, such as CMs and neurons, to increase tissue renewal in humans is a goal of regenerative medicine. Our findings reveal that adult, post-mitotic differentiated cells can be partially reprogrammed to a more renewable phenotype (Fig. 7). New CMs coupled to existing CMs and had contractile function indicating that they productively integrated into existing myocardium. Our findings suggest that induced tissue renewal may be useful to treat degenerative human disease such as HF.

YAP5SA induces adult cardiomyocyte reversion to a primitive, fetal-like cell state

Developing and postnatal CMs are proliferative but still must perform a contractile function to maintain viability of the organism. In developing CMs, this is accomplished by transient sarcomere breakdown and re-assembly (Ahuja et al., 2004). Although YAP5SA OE mice die soon after YAP5SA induction, YAP5SA OE CMs appear to balance proliferative capacity while maintaining contractile function to some extent. We see reversion of chromatin accessibility to a fetal-like CM state and a YAP-TEAD-AP-1 driven genetic program that has similarities to that of an E14.5 CM. Our data suggest that YAP5SA is dynamically regulated in the CM since many YAP5SA OE CMs had very high nuclear YAP5SA expression but other YAP5SA OE CMs had lower nuclear expression.

Our findings provide insight into how developmental pathways may function in the adult heart. For example, *Wntless* and *Noggin* are regulators of two developmental signaling pathways, WNT and Bone morphogenetic (BMP) signaling that have been studied in development but much less is known in the adult heart (Deb, 2014; Tzahor, 2007; Wang et al., 2011). Wntless is essential for trafficking and secretion of all WNT ligands suggesting that Yap promotes expression of WNT ligands (Ching and Nusse, 2006). Previous work has connected Hippo-YAP to WNT signaling through several mechanisms (Piccolo et al., 2014). Supplementation with Noggin, a BMP inhibitor, improved cardiac function after ischemia

reperfusion injury in adult mice (Pachori et al., 2010). It will be important to thoroughly investigate Noggin and Wntless in CM renewal.

YAP5SA lineage cardiomyocytes integrate into the heart

Our data suggest that newly born YAP5SA OE adult CMs can productively incorporate into existing myocardium. YAP5SA OE CMs contract efficiently, conduct action potentials, and couple to existing CMs. These findings, along with the observation that some YAP5SA CMs have relatively low levels of nuclear YAP5SA, suggest that YAP5SA is negatively regulated through Hippo independent mechanisms. Vital imaging experiments revealed that Yki, the Drosophila orthologue of YAP and TAZ, dynamically cycles between the nucleus and cytoplasm (Manning et al., 2018). YAP5SA may also cycle from nucleus to other subcellular locations in the CM as a negative regulatory mechanism.

While there is no precedent for integration of newly generated adult CMs into existing myocardium, the example of adult neurogenesis is instructive. In adult murine olfactory bulb, newly born neurons integrate into existing synaptic circuitry through a defined developmental progression that depends on external stimuli to promote survival of new neurons (Ming and Song, 2005). It is unclear how YAP5SA OE CMs integrate into the existing myocardium, however, the YAP5SA model will be a valuable resource to investigate this problem.

Incorporation of YAP5SA CMs into the heart may be facilitated by mechanisms inhibiting YAP5SA nuclear activity. YAP5SA induces a negative feedback loop that functions through multiple mechanisms to inhibit YAP. In addition to induction of *Lats2* transcription, a direct YAP target that will not inhibit YAP5SA, we see strong up-regulation of *VGLL2, VGLL3,* and *VGLL4* genes that encode competitive inhibitors of the YAP-TEAD interaction. Additionally, YAP5SA activity can be inhibited by ICD proteins, such as α-catenins, or actin binding proteins such as AMOT family proteins, which are both direct YAP targets and YAP interacting proteins (Li et al., 2015a; Morikawa et al., 2017; Ragni et al., 2017).

Chromatin accessibility contributes to the differentiated state of cardiomyocytes

We propose a model where the adult CM phenotype is maintained by decommissioned enhancers that are made newly accessible by YAP5SA. It has been shown that cardiac differentiation during development is accompanied by gradual reduction of chromatin accessibility at developmental loci (Stergachis et al., 2013). As ES cells differentiate into CMs, there is a rearrangement of chromatin accessibility with loss of accessible chromatin containing binding elements for pluripotency factors, and gain in accessible MEF2 and NKX2.5 elements that define the CM phenotype (Stergachis et al., 2013). This rearrangement of chromatin accessibility is considered irreversible except in pathologic states, such as cancer, where developmental enhancers are co-opted, often from multiple cell lineages (Stergachis et al., 2013). Our data indicate that chromatin accessibility can be manipulated in a productive way to promote tissue renewal.

YAP, ploidy and cell cycle progression

Many YAP5SA target genes encoding cell cycle regulators are already accessible. This is consistent with previous work revealing that YAP activates transcription of some target genes through transcriptional pause release (Galli et al., 2015). Based on our observations, revealing increased accessibility of developmental enhancers during YAP5SA-dependent proliferation, many other genes important for *bona fide* proliferation, such as cytoskeletal genes that are important for productive cell division, are repressed by chromatin compaction.

There is evidence that a subpopulation of smaller, mononucleated diploid CMs is more prone to complete cell division in mice (Patterson et al., 2017). We found an increase in the proportion of mononucleated CMs after YAP5SA induction, and YAP5SA OE CMs were smaller than control CMs. However, it is still unclear that the mononucleated diploid phenotype is required for successful proliferation. For example, bi-nucleated hepatocytes contribute to liver regeneration (Miyaoka et al., 2012). Intriguingly, YAPS127A has been shown to induce proliferation of tetraploid hepatocytes *in vivo* (Ganem et al., 2014). Future studies, using the YAP5SA model, can more definitively address the predisposition of different populations of CMs towards proliferation and the role of ploidy in these events.

It is hypothesized that a structural block prevents CMs from proliferating. If this is the case, YAP5SA overcomes the CM structural cell cycle checkpoint. It has been shown that the structural cell cycle checkpoint in CMs can be overcome while shutting down expression of genes associated with myocyte maturation (Tzahor and Poss, 2017). We observed that the MEF2A motif was decommissioned in YAP5SA OE CMs. MEF2A is maintains the mature CM phenotype (Naya et al., 2002). YAP5SA OE CMs also show evidence of sarcomeric disassembly. Since CMs turn over their contractility protein apparatus continually (Willis et al., 2009), it is conceivable that CM renewal occurs while the contractile machinery is transiently down-regulated in YAP5SA OE CMs similar to zebrafish CMs (Jopling et al., 2010). Our findings suggest that careful manipulation of the Hippo-YAP pathway may be useful for promoting adult tissue renewal for medical benefit.

STAR Methods

CONTACT FOR REAGENT AND RESOURCE SHARING

Further information and requests for resources and reagents may be directed to and will be fulfilled by the Lead Contact, James Martin (jfmartin@bcm.edu).

EXPERIMENTAL MODEL AND SUBJECT DETAILS

Mouse studies were performed in accordance with the institutional animal care and use committee at Baylor College of Medicine (Houston, TX, USA). The pCMV-Flag YAP2 5SA sequence, a gift from Kun-Liang Guan (Addgene, Cambridge, MA, USA, plasmid # 27371) (Zhao et al., 2007), was cloned into the CAG-loxP-eGFP-Stop-loxP-IRES-βGal expression construct. The DNA sequence encodes a human variant of YAP that has a total of eight serine (S) residues mutated to alanine (A) at the five canonical Lats-dependent phosphorylation motifs (S61A, S109A, S127A, S128A, S131A, S163A, S164A, and S381A). This version of YAP excludes exon 6 and therefore includes a predicted leucine

zipper that can enhance transactivation (Finch-Edmondson et al., 2016). We established a line of YAP5SA overexpressing (OE) mice (Tg[Jojo-Flag::YAP5SA]5JFM) by performing the pronuclear injection of linearized DNA encoding the YAP transgene (Fig. 1A) into fertilized oocytes from FVB/N mice, which were then implanted into pseudopregnant females. Single crosses were performed with homozygous αMyHC-Cre-ERT2 mice (Referred to as "MCM" mice), which were maintained on the C57Bl/6J background. All control animals were littermates or age-matched if littermates were unavailable. Genotype was determined both by visualizing enhanced green fluorescent protein (eGFP) expression in the tail skin and by performing PCR genotyping (F: AAGCCTTGACTTGAGGTTAG, R: CGTCATCGTCTTTGTAGTCC). All experiments involving adult mice were performed with male or female mice that were 7 to 12 weeks of age. No difference between sexes was observed in any cardiac phenotype. Tamoxifen induction of Cre was accomplished by performing standard intrapleural injections of tamoxifen (40μg/g) daily for four days in the high dose, or a single 20μg/g low dose where indicated. Tamoxifen was prepared in corn oil.

METHOD DETAILS

Western Blotting—Western blotting was performed using standard methods with lysates prepared by homogenizing hearts with a bead homogenizer in buffer with HEPES, EDTA, and Triton. The lysates, after 5 minutes boiling in a reducing tris-based sodium dodecyl sulfate (SDS) sample buffer (80 μg/well), were loaded into acrylamide gels and ran at 120 volts for a sufficient time to achieve separation. Proteins were then transferred to PVDF membranes and imaged by using the Li-COR Odyssey imaging system (LI-COR Biosciences). Primary antibodies were as follows: rabbit anti-YAP (1:1000), Novus Biologicals Cat#NB110-583538; mouse anti-M2Flag (1:1000), Sigma-Aldrich Cat#F1804; mouse anti-GAPDH (1:5000), Millipore Cat#CB1001; anti-P-YAP (S127, mouse homolog S112) (1:1000), Cell Signaling Technologies Cat#4911. Fluorescent secondary antibodies were goat anti-rabbit IgG and goat anti-mouse IgG (1:5000), LI-COR Cat#925-68071 & Cat#925-32210. Quantitation was performed by using the gel analysis feature in Fiji (ImageJ) (National Institutes of Health, Bethesda, MD, USA).

Ultrasound Echocardiography—M- and B-mode echocardiography were performed according to established protocols at the Baylor College of Medicine Mouse Phenotyping Core using a 30 MHx scanhead (RMV7007B) on a VisualSonics 770 system, and analyzed using Vevolab 2.2.0 software (Fujifilm Visualsonics).

Left Ventricular (LV) Size and Number of CMs—To determine the total number of cardiomyocytes in each left ventricle by stereology 48 hours after tamoxifen, we first excised the hearts of mice and fixed them in diastole by performing retrograde perfusion with 30mM KCl followed by 10% formalin, and then drop-fixing them in 10% formalin. The hearts were embedded in paraffin and cut from the apex to the aorta into 7-micron sections. We then computed the volume of the left ventricle in each heart by plotting the area of the LV myocardium on a microscope slide as a function of tissue depth and then integrated the area under the curve. From that volume, we computed the ratio of LV weight to body weight by converting the volume of the LV to mass by using the density of muscle (1.053 g/mL)(Vinnakota and Bassingthwaighte, 2004). The 7-micron sections at various

tissue depths were then stained with anti–PCM-1 (Sigma-Aldrich Cat#HPA023370), DAPI, and Rhodamine-conjugated wheat germ agglutinin (WGA, Vector Labs Cat#RL-1022) to label CM nuclei, all nuclei, and cell borders, respectively. We then used confocal microscopy to image through the entire thickness of each section and count the number of PCM-1(+) nuclei in the imaging frame. Partial nuclei on the bottom and left edges of the frame were not counted, whereas partial nuclei on the top and right edges were counted. Z-stacks were acquired at random throughout sections from different tissue depths (40 Z-stacks/heart). Nuclei were counted only if they were both PCM-1(+) and DAPI(+), with PCM-1 encircling the DAPI-stained area (Fig. 2P). To calculate the total number of CMs, the number of nuclei counted per volume was computed to a nucleation density, which was then extrapolated to the entire volume of the myocardium and then corrected for the average nucleation of the myocytes from each genotype (control: 2.04 nuclei/CM; YAP5SA OE: 1.92 nuclei/CM, Fig. S1J), as described elsewhere (Bruel and Nyengaard, 2005). The person quantifying the images was blinded to genotypes.

Flow Cytometry Analysis of DNA Content—CM nuclei were isolated as previously described (Richardson, 2016). EdU was administered in sterile saline, 100μg/g mouse by intrapleural injection. Hearts were dissected and minced on ice into 15mL Cell Lysis Buffer (0.32M sucrose; 10mM Tris-HCl (pH 8); mM CaCl2; 5mM magnesium acetate; 2.0mM EDTA; 0.5mM EGTA; 1 mM DTT) and with a Biogen Series PRO200 (PRO Scientific) homogenizer, and then in a dounce homogenizer with another 15mL (30 total) of Cell Lysis Buffer. After 100μm filtration, nuclei were pelleted at 700G and resuspended into 25mL Sucrose Gradient Solution (2.1M sucrose; 10mM Tris-HCl (pH 8); 5mM magnesium acetate 1mM DTT), which was then placed on on top of 10mL fresh Sucrose Gradient Solution in an ultracentrifuge tube. That tube was then spun at 13,000G for 1 hour. After centrifugation, the nuclear pellet was resuspended into 1.3mL Nuclei Storage Buffer (0.44M sucrose; 10mM Tris-HCl (pH 7.2); 70mM KCl; 10mM MgCl2; 1.5mM spermine). Antibody negative control 0.3mL was then removed, and the remaining 1mL was incubated with anti-PCM1 (8μg/mL). The isotype control and antibody-containing mixtures were incubated overnight at 4°C and centrifuged at 700G for 10 minutes to pellet and wash with Nuclei Storage Buffer. PCM-1-bound nuclei were then conjugated to fluorescent secondary antibodies and, and EdU was identified using the Click-it EdU Flow Cytometry Assay Kit per manufacturer's instructions (Thermo Fisher Scientific, Cat#C10340). DNA content was quantified by DAPI fluorescence. Detection was performed using a BD FACSAria ii (BD Biosciences), and data were analyzed in FlowJo software (Tree Star). Gating was based on isotype controls and fluorophore-negative controls. Flow cytometry was performed at the Texas Heart institute Flow Cytometry Core Facility.

Single Cell Morphology and Physiology—The day after the fourth tamoxifen injection, cardiomyocytes were isolated by performing retrograde perfusion of digestion buffer (Reynolds et al., 2016), along with mechanical shearing. Briefly, the hearts were removed from mice, and then perfused in retrograde with 37°C pH 7.4 HEPES-Tyrode's buffer (130mM NaCl; 5.4 mM KCl; 0.5mM MgCl; 0.33 mM NaH_2PO_4; 0.25mM HEPES; 22mM Glucose) containing collagenase (Collagenase A, Sigma Cat#10103586001) using the Langendorff method. Hearts were then mechanically sheared and filtered through a

200μm mesh filter for a single-cell suspension. For immunocytochemistry and cell size measurements, freshly isolated cells were washed in calcium-free PBS, fixed in 10% formalin for 10 minutes, and then permeabilized with 0.5% Triton 100. Cell size was quantified by capturing static images of plated cells (Nikon Eclipse 80i microscope, equipped with a Nikon DSFi1 camera) and outlining them in ImageJ (National Institutes of Health, Bethesda, MD, USA) to quantify the 2-dimensional profile area of cardiomyocytes. The person quantifying the images was blinded to genotypes. Live physiologic imaging was performed by using an IonOptix Myocyte Calcium and Contractility Recording System (IonOptix, Westwood, MA, USA). Isolated cardiomyocytes were removed from collagenase by low speed centrifugation (300RPM), and then resuspended and plated on glass in 1.8 mM Ca^{2+}-containing Tyrodes solution. Cells were selected for absent or minimal GFP (post-recombination), and were field-stimulated by using a MyoPacer (IonOptix) at 20 V/cm. Sarcomere shortening was quantified by performing Fourier transform of the sarcomere periodicity by using the Ionoptix IonWizard software during the final 20 seconds of a two-minute 1-Hz pacing protocol.

Histology & Immunofluorescence—Freshly dissected embryos and postnatal hearts were dissected and imaged for endogenous GFP fluorescence by using a Zeiss SteREO Discovery.V12, equipped with a Zeiss AxioCam Hrc.

For fixation, hearts were retrogradely perfused with cardioplegic 20 mM KCl-PBS before perfusing them with 10% neutral buffered formalin, followed by embedding in paraffin. Transverse sections (7 microns) were cut and mounted onto charged polylysine slides. A portion was stained with Masson's trichrome stain or Picrosirius Red staining. Immunohistochemistry (Fig. 2E,P, Fig. S1F, Fig. S2E) was performed by first deparaffinizing and rehydrating sections, followed by antigen retrieval and permeabilization in 0.1% tween-20 in PBS. Sections were blocked (10% donkey serum in phosphate-buffered saline [PBS], 0.1% tween-20) and then incubated with primary and secondary antibodies (all separately, in succession at 4 degrees C) overnight before imaging. (Fig. 2E Mouse anti-AuroraKB, Novus Cat#NBP2-50039; anti-Mouse Alexa 488, Thermo Fisher Scientific Cat#A-21202) (Fig. 2P rabbit Anti-PCM-1, Sigma-Aldrich Cat#HPA023370; anti-rabbit Alexa 647, Thermo Fisher Scientific Cat#A-31573) (Fig. S1F. rabbit DYKDDDDK Tag Antibody, Cell signaling technology Cat#2368; anti-rabbit Alexa 488, Thermo Fisher Scientific Cat#A-21206) (Fig. S2E rabbit anti-N-cadherin, anti-rabbit Alexa 647; chicken anti-β-gal, Abcam Cat#ab9361; anti-chicken Alexa 488, Thermo Fisher Scientific Cat#A-11039). Nuclei were stained with DAPI (4',6-diamidino-2-phenylindole). EdU (5-ethynyl-2'-deoxyuridine) staining was performed by using Click-it technology *via* Thermo Fisher Scientific's Click-it Alexa Fluor 647 imaging kit (Cat#C10340). Rhodamine-conjugated WGA used was from Vector labs Cat#RL-1022. The person quantifying the images was blinded to genotypes. All imaging was performed with a Zeiss LSM 780 confocal microscope in the Optical Imaging and Vital Microscopy Core at Baylor College of Medicine (Houston, TX, USA).

For frozen sections (Fig. 2C,I. Fig. S1H,I), hearts were extracted, perfused with a 30% sucrose and 20 mM KCl-PBS solution, and then placed into Tissue-Tek optical cutting temperature (OCT) compound (V.W.R. Cat#25608-930) before freezing over dry ice.

Sections (7 microns) were then cut and mounted on glass slides. For immunofluorescence staining, antigen retrieval was performed by warming the sections to 42°C and then placing them in acetone at −20°C for 20 minutes before blocking with 10% serum. Sections were then incubated with primary and secondary antibodies (all separately, in succession at 4 degrees C) overnight before imaging. (Fig. 2C rat anti-PHH3, Abcam Cat#ab10543; anti-rat Alexa 488, Thermo Fisher Scientific Cat#A-11006; Mouse anti-cTnT-Alexa-647 conjugate, BD Pharmingen cat#565744). BrdU staining was performed after acetone treatment by hydrolyzing DNA with 1N HCl for 50 minutes at 37 degrees C, and otherwise proceeding as usual. (Fig. 2I rat anti-BrdU, Accurate Chemical & Scientific corp. Cat#OBT0030; anti-rat Alexa 488, Thermo Fisher Scientific Cat#A-11006) (Fig. S1H rat anti-BrdU, Accurate Chemical & Scientific corp. Cat#OBT0030; anti-rat Alexa 488, Thermo Fisher Scientific Cat#A-11006; rabbit Anti-PCM-1, Sigma-Aldrich Cat#HPA023370; anti-rabbit Alexa 546, Thermo Fisher Scientific Cat#A-10040) (Fig. S1I rat anti-BrdU, Accurate Chemical & Scientific corp. Cat#OBT0030; anti-rat Alexa 488, Thermo Fisher Scientific Cat#A-11006; mouse anti-cTnT, Thermo Fisher Scientific Cat#MA5-12960; anti-mouse Alexa 546, Thermo Fisher Scientific Cat#A-10036). EdU (5-ethynyl-2'-deoxyuridine) staining was performed by using Click-it technology *via* Thermo Fisher Scientific's Click-it Alexa Fluor 647 imaging kit (Cat#C10340). Rhodamine-conjugated WGA used was from Vector labs Cat#RL-1022. Nuclei were stained with DAPI. The person quantifying the images was blinded to genotypes. All imaging was performed with a Zeiss LSM 780 confocal microscope in the Optical Imaging and Vital Microscopy Core at Baylor College of Medicine.

Immunocytochemistry (Fig. 1I,2A) was performed according to standard protocols. Briefly, Langendorff-isolated CMs were fixed for 10 minutes at room temperature in 10% formalin. After permeabilizing the CMs with 0.5% triton-100 for 20 minutes and blocking with 2% fetal bovine serum (FBS) and 2% bovine serum albumin (BSA), antibodies were incubated (separately, in succession) overnight before imaging (primary: rabbit anti-YAP [1:200], Novus Cat#NB110-583538; mouse anti-cTnT [1:200] Thermo Fisher Scientific Cat#MA5-12960; secondary: anti-rabbit, Alexa 647 Thermo Fisher Scientific Cat#A-31573; anti-mouse, Alexa 546, Thermo Fisher Scientific Cat#A-10036). EdU (5-ethynyl-2'-deoxyuridine) staining was performed by using Click-it technology *via* Thermo Fisher Scientific's Click-it Alexa Fluor 647 imaging kit (Cat#C10340). *Bona fide* presence of EdU in individual cardiomyocytes was determined by acquiring confocal z-stacks. Nucleation was quantified in these isolated cardiomyocytes by staining with DAPI and counting the number of nuclei per cell by confocal Z-stacks. The person quantifying the images was blinded to genotypes. All imaging was performed with a Zeiss LSM 780 confocal microscope.

EdU, BrdU Double Labeling Analysis—Low dose tamoxifen (1 injection, 20μ9/9) EdU, BrdU double labeling analysis was as follows: Given the percentages of EdU(+) and BrdU(+) cells, we know the probability of a cardiomyocyte entering S-phase in one of those time periods to be 4.25% and 5.04%, respectively. If all CMs are equivalent, one would predict 0.21% of the cells would be labeled during both times. However, 0.83% of the cells

were positive. This suggests that there is a subset of cells more prone to cycling than others. Statistically, the presence of BrdU is not an independent event from the presence of EdU.

Optical Mapping—Mice were anesthetized with isoflurane to the surgical plane of anesthesia, and heparin was injected intraperitoneally (100 units) before cervical dislocation. The heart was then removed and washed in cold, oxygenated (95% O_2, 5% CO_2) Tyrode's solution (137mM NaCl; 5.4mM KCl; 1mM MgCl2; 5 mM HEPES; 10 mM glucose; 3 mM NaOH; 2.5mM Ca^{2+}; pH 7.4). The aorta was cannulated with a 21-gauge cannula, and the heart was retrogradely perfused with Tyrode's solution, maintaining aortic pressure between 80 and 120 mmHg. An electrode (Harvard Apparatus) was placed on the surface of the right atrium for pacing stimulations (10 Hz, 12 Hz, and 14 Hz) generated by PowerLab 26T (ADInstruments). To eliminate contractile artifacts, hearts were loaded with blebbistatin (Sigma-Aldrich, B0560-5 mg, 50 μl of 2.5 mg/ml in dimethyl sulfoxide [DMSO]). We then perfused the hearts with the voltage-sensitive dye di-4-ANEPS (Invitrogen, D-1199, 20 μl of 2.5 mg/ml in DMSO). An LED light was used for excitation (wavelength, 530 nm). Fluorescence emission, signifying Vm, was long-pass filtered (>590nm, 590FG05-50, Andover Corporation, Optical Filter) and measured with a MiCAM0 CMOS camera (SciMedia). Surface electrocardiograms (ECGs) (ADInstruments) were monitored during experiments by using LabChart. Conduction velocities and activation maps were calculated with Rhythm software(Laughner et al., 2012) .

In Vivo Electrophysiology—As previously described (Wang et al., 2014), we recorded ECGs continuously for 5 days spanning the YAP5SA OE induction protocol and one day later. We used telemetry transmitters (Data Sciences International) implanted in the abdominal cavity of ambulatory mice. The saturated calomel electrodes were placed in a lead II configuration, and ECGs were recorded by using version 4.1 Dataquest software. T-wave measurements were performed by computing the area under the curve.

Nuclear Isolation for Sequencing—Nuclear isolation was performed as previously described, with the following specifications (Mo et al., 2015): Briefly, fresh cardiac tissue was harvested on ice and was immediately homogenized with a Biogen Series PRO200 (PRO Scientific) before performing Dounce homogenization in HB buffer (0.25M sucrose, 25mM KCl, 5mM MgCl2, 20mM Tricine-KOH, pH 7.8; with protease inhibitors; 1mM DTT; 0.15mM Spermine; 0.5mM Spermidine, and RNAse inhibitors) with 5% IGEPAL CA-630. Nuclei were isolated via density gradient centrifugation with optiprep density gradient medium after mixing homogenate 1:1 with a 50 iodoxinal (5 volumes Optiprep [Sigma-Aldrich, Cat#D1556] with 1 volume Diluent [150mM KCl; 30mM $MgCl_2$; 120mM Tricine-KOH; pH 7.8]) . After 18 minute 10,000G centrifugation, all nuclei isolated from a 30% to 40% interface were precleared with Protein-G Dynabeads (Thermo Fisher Scientific, Cat#10004D). Next, nuclei were immunoprecipitated with an anti–PCM-1 (Sigma-Aldrich, Cat#HPA023370) antibody and Protein-G Dynabeads (washing 7 times with Buffer HB with 0.4% IGEPAL CA-630) to enrich for CM nuclei as described previously (Gilsbach et al., 2014).

RNA-sequencing—RNA from bead-bound PCM-1(+) nuclei was collected by using the RNEasy Plus Micro kit (Qiagen, Hilden, Germany). Nuclear RNA sequencing (RNA-seq) libraries were constructed by using the Stranded RNA-seq Kit with Ribo Erase (Kapa Biosystems Inc.) with custom Y-shaped adapters. Paired-end 2×75 bp sequencing was performed for RNA-seq libraries with an Illumina Nextseq instrument (DNA Link). Reads were first mapped to the mouse genome (mm10) by using STAR (Dobin et al., 2013). Differential expression analysis was then carried out with DESeq2 (Love et al., 2014). Gene ontology analysis was performed by using Metascape [http://metascape.org] (Tripathi et al., 2015), and displayed using GOplot (Walter et al., 2015). Gene set enrichment analysis using publicly available data(Uosaki et al., 2015) was performed by interrogating the top 200 most enriched transcripts in either adult hearts relative to embryonic (E12-14); or embryonic relative to adult against our RNA-seq dataset (enrichment score is relative to control) (Mootha et al., 2003; Subramanian et al., 2005; Uosaki et al., 2015).

ATAC-sequencing—Approximately 50,000 bead-bound PCM-1(+) CM nuclei were used as input for the assay for transposase accessible chromatin with high throughout sequencing (ATAC-seq). ATAC-seq libraries were generated as previously described (Buenrostro et al., 2013). Paired-end 2×75 bp sequencing was performed with an Illumina Nextseq instrument (DNA Link Inc.). Reads were mapped to the mouse genome (mm10) by using Bowtie2 with default paired-end settings (Langmead et al., 2009). Next, all non-nuclear reads and improperly paired reads were discarded. Duplicated reads were removed with Picard-MarkDuplicates. Peak calling was carried out with MACS2 (callpeak–nomodel–broad). Blacklisted regions were lifted over from mm9 to mouse genome mm10 and removed along with peaks of low sequencing quality (>q30 required). Reads were counted for each condition from the comprehensive peak file (YAP5SA OE and control replicates merged) by using bedtools (multicov module) (Quinlan, 2014). Quantile normalization of ATAC-seq data sets was performed with CQN (Hansen et al., 2012), and offsets were fed into DESeq2 to quantify differential accessibility (Love et al., 2014). Nucleosome calling was carried out with NucleoATAC (Schep et al., 2015). Motif enrichment analysis was conducted with HOMER (Heinz et al., 2010) (findMotifsGenome.pl and annotatePeaks.pl). Gene tracks were shown by using the UCSC genome browser. ES cell ATAC-seq data was used from GSM1563569, with reads mapped to the mm10 genome using bowtie2 and analyzed with HOMER (annotatePeaks.pl) and Galaxy/deeptools2 (multiBigwigSummary, plotCorrelation) (Ramirez et al., 2016).

H3K27Ac ChIP-seq Data Aquisition—H3K27Ac Chip-seq from developing mouse hearts was analyzed from available data (GSM1264374, GSM1264384) (Nord et al., 2013) and were mapped to the mouse genome (build mm10) by using Bowtie2 default parameters (Nord et al., 2013). Gene tracks were shown by using the UCSC genome browser, and reads were plotted using HOMER (annotatePeaks.pl).

H3K27Ac Chip-seq from mice with hypertrophic stimulus (1 week after aortic constriction), or in heart failure (8 weeks after aortic constriction) was retrieved from the GEO database (GSM2497652 & GSM2687477 in GSE95143)(Nomura et al., 2018). We then visualized our YAP5SA OE and Control ATAC-seq data globally at regions with non-overlapping

H3K27Ac ChIP-seq peaks ($p < 1e^{-5}$) between 1 week after aortic constriction and 8 weeks after using HOMER (annotatePeaks.pl). Conversely, we visualized H3K27Ac ChIP-seq reads from 1 week post aortic constriction and 8 weeks post aortic constriction at control or YAP5SA-specific ATAC-seq peaks ($P < 0.035$). Reads from the mm9 genome were converted to mm10 using CrossMap (CrossMap.py).

Heart Failure RNA-Seq Data Acquisition—We retrieved RNA-seq data on mice in heart failure due to dilated cardiomyopathy secondary to aortic constriction vs sham-operated healthy adults from the GEO database (GSE112055) (Kokkonen-Simon et al., 2018) (n = 5 sham, 5 heart failure). Differential gene expression was performed the same way our YAP5SA vs control RNA-seq data was analyzed using DESeq2 on 5 replicates/group (Sham 1-5 and TAC 1-5).

YAP ChIP-seq Data Incorporation—YAP ChIP-seq data was used from GSM2220157 (Croci et al., 2017) and mapped to mm10 using LiftOver (https://genome.ucsc.edu/cgi-bin/hgLiftOver). Control and YAP5SA OE ATAC-seq reads, centered at YAP ChIP-seq peaks were plotted as heat maps and profile plots using deepTools3 (plotProfile). Motif discovery analysis was performed using HOMER (findMotifsGenome.pl). YAP ChIP-seq targets in our RNA-seq data set were determined by taking YAP ChIP-seq peaks that contained open TEAD motifs (ATAC-seq average normalized read depth > 2 over the peak length).

Chromosome Conformation Capture (3C & 4C)—3C was performed using methods described previously with minor modifications (Hagege et al., 2007). First, CM nuclei were isolated by PCM-1 immunoprecipitation as with the ATAC-seq and RNA-seq experiments. For most assays, nuclei were digested with BgIII restriction enzyme (NEB), whereas for Nog and Wls loci analyses, nuclei were digested with EcoRI (NEB) or BsrG1 (NEB) respectively. Digested chromatin was highly diluted and ligated with T4 DNA ligase (NEB). DNA fragments were de-crosslinked overnight at 65C, then treated with Proteinase K and RNAse A. DNA was then purified via phenol/chloroform extraction and ethanol precipitation. 3C templates were used to perform semiquantitative PCR (Actb loading standard) with iTaq™ Universal SYBR® Green Supermix (Bio-Rad, Cat#1725120). Primers flanked the restriction sites located close to gene promoters and putative enhancers. Data are presented as the ratio of amplification obtained from 3C templates normalized to Control CM enhancer-promoter crosslinking for each individual gene. Approximately 3 million CM nuclei per preparation were used for 3 preparations from a total of 6 mice per group. Controls were a mixture of Tamoxifen-injected MCM mice and YAP5SA/MCM mice without tamoxifen. Each preparation was then used to perform 3 technical qPCR replicates/preparation/qPCR reaction. The average of the qPCR technical replicates from each 3C preparation was then used for averaging and SEM with the other 3C preparations for n=3/group.

For 4C, approximately 5 million bead-bound PCM-1-enriched cardiomyocyte nuclei from 6 mice, isolated as described above for 3C, were used as input for two replicates. The 4C protocol was performed as described previously (van de Werken et al., 2012), with minor modifications. The first restriction enzyme digestion was performed with DpnII (NEB, Cat#R0543M). The first ligation was perfomed overnight with T4 DNA ligase (Roche,

Cat#10799009001). Samples were then de-crosslinked with Proteinase K (Thermo Fisher, Cat#EO0491) overnight. DNA was purified using P-beads from the NucleoMag 96 PCR kit (Macherey-Nagel, Cat#744100.1). The second enzymatic digestion was performed overnight with Csp6I (Thermo Fisher, Cat#ER0211). Samples were then ligated, as described above, overnight and purified with NucleoMag P-beads. We then employed a 2-step PCR protocol to amplify DNA and generate libraries for sequencing. All PCR reactions were carried out with Expand Long template polymerase (Roche, Cat#11681842001). Libraries were purified using Agencourt AMPure XP beads (Beckman Coulter, Cat#A63881), at 0.8X. Finally, all libraries were sequenced on an Illumina Nextseq 500.

QUANTIFICATION AND STATISTICAL ANALYSIS

All statistical tests, error bars, P-values, and n numbers are reported in the corresponding figure legends. Researchers were blinded to genotype during the acquisition and processing of data. Sample sizes were not pre-determined, but were chosen based on previous publications. Mice were pre-determined to be excluded only if they had obvious anatomical or health abnormalities prior to genetic manipulation; One case was observed where a YAP5SA mouse we intended to use for optical mapping was not used due to severely stunted growth. To address randomness, any available (mutant or control) mice were included in the study. Control mice are indicated in the figure legends. They were tamoxifen-injected MCM mice; transgenic YAP5SA/MCM mice without tamoxifen; or MCM mice without tamoxifen. Controls were littermates with or age-matched to experimental mice. No differences in variances were detected between any group in the reported experiments. One-way, two-tailed analysis of variance tests (ANOVA), followed by post-hoc tests were computed in Origin Pro (OriginLab Corporation). Fisher's exact tests, Chi-squared test, and Mantel-Cox tests were performed in Prism 5 (GraphPad). All graphs were generated in R or Microsoft Excel and presented using Inkscape. Cartoons were also created in Inkscape (http://www.inkscape.org/; https://www.R-project.org/.

DATA AND SOFTWARE AVAILABILITY

The ATAC-seq, RNA-seq, and 4C-seq data have been deposited at the Gene Expression Omnibus under the ID code GSE123457

Supplementary Material

Refer to Web version on PubMed Central for supplementary material.

Acknowledgements

Supported by Intellectual and Developmental Disability Research Center grant (1U54 HD083092) Eunice Kennedy Shriver NICHD; Baylor College of Medicine Mouse Phenotyping Core NIH (U54 HG006348); NIH (DE 023177, HL 127717, HL 130804, and HL 118761 (J.F.M.); HL 089898, HL 091947, HL 117641, HL 129570 (X.H.T.W.); AR 061370 (G.G.R.); F31HL136065 (M.C.H.); Vivian L. Smith Foundation, MacDonald Research Fund Award 16RDM001, and LeDucq Foundation Transatlantic Networks of Excellence Cardiovascular Research 14CVD01: "Defining genomic topology of atrial fibrillation." (J.F.M.).

References

Ahuja P, Perriard E, Perriard JC, and Ehler E (2004). Sequential myofibrillar breakdown accompanies mitotic division of mammalian cardiomyocytes. Journal of cell science 117, 3295–3306. [PubMed: 15226401]

Alkass K, Panula J, Westman M, Wu TD, Guerquin-Kern JL, and Bergmann O (2015). No Evidence for Cardiomyocyte Number Expansion in Preadolescent Mice. Cell 163, 1026–1036. [PubMed: 26544945]

Bergmann O, Zdunek S, Felker A, Salehpour M, Alkass K, Bernard S, Sjostrom SL, Szewczykowska M, Jackowska T, Dos Remedios C, et al. (2015). Dynamics of Cell Generation and Turnover in the Human Heart. Cell 161, 1566–1575. [PubMed: 26073943]

Bersell K, Arab S, Haring B, and Kuhn B (2009). Neuregulin1/ErbB4 signaling induces cardiomyocyte proliferation and repair of heart injury. Cell 138, 257–270. [PubMed: 19632177]

Bersell K, Choudhury S, Mollova M, Polizzotti BD, Ganapathy B, Walsh S, Wadugu B, Arab S, and Kuhn B (2013). Moderate and high amounts of tamoxifen in alphaMHC-MerCreMer mice induce a DNA damage response, leading to heart failure and death. Disease models & mechanisms 6, 1459–1469. [PubMed: 23929941]

Bruel A, and Nyengaard JR (2005). Design-based stereological estimation of the total number of cardiac myocytes in histological sections. Basic research in cardiology 100, 311–319. [PubMed: 15795797]

Buenrostro JD, Giresi PG, Zaba LC, Chang HY, and Greenleaf WJ (2013). Transposition of native chromatin for fast and sensitive epigenomic profiling of open chromatin, DNA-binding proteins and nucleosome position. Nature methods 10, 1213–1218. [PubMed: 24097267]

Ching W, and Nusse R (2006). A dedicated Wnt secretion factor. Cell 125, 432–433. [PubMed: 16678089]

Croci O, De Fazio S, Biagioni F, Donato E, Caganova M, Curti L, Doni M, Sberna S, Aldeghi D, Biancotto C, et al. (2017). Transcriptional integration of mitogenic and mechanical signals by Myc and YAP. Genes & development 31, 2017–2022. [PubMed: 29141911]

Dai X, Liu H, Shen S, Guo X, Yan H, Ji X, Li L, Huang J, Feng XH, and Zhao B (2015). YAP activates the Hippo pathway in a negative feedback loop. Cell research 25, 1175–1178. [PubMed: 26315483]

Deb A (2014). Cell-cell interaction in the heart via Wnt/beta-catenin pathway after cardiac injury. Cardiovascular research 102, 214–223. [PubMed: 24591151]

Denny SK, Yang D, Chuang CH, Brady JJ, Lim JS, Gruner BM, Chiou SH, Schep AN, Baral J, Hamard C, et al. (2016). Nfib Promotes Metastasis through a Widespread Increase in Chromatin Accessibility. Cell 166, 328–342. [PubMed: 27374332]

Dobin A, Davis CA, Schlesinger F, Drenkow J, Zaleski C, Jha S, Batut P, Chaisson M, and Gingeras TR (2013). STAR: ultrafast universal RNA-seq aligner. Bioinformatics (Oxford, England) 29, 15–21.

Felix M, Chayengia M, Ghosh R, Sharma A, and Prasad M (2015). Pak3 regulates apical-basal polarity in migrating border cells during Drosophila oogenesis. Development 142, 3692–3703. [PubMed: 26395489]

Finch-Edmondson ML, Strauss RP, Clayton JS, Yeoh GC, and Callus BA (2016). Splice variant insertions in the C-terminus impairs YAP's transactivation domain. Biochemistry and biophysics reports 6, 24–31. [PubMed: 28018981]

Frisen J (2016). Neurogenesis and Gliogenesis in Nervous System Plasticity and Repair. Annual review of cell and developmental biology 32, 127–141.

Galli GG, Carrara M, Yuan WC, Valdes-Quezada C, Gurung B, Pepe-Mooney B, Zhang T, Geeven G, Gray NS, de Laat W, et al. (2015). YAP Drives Growth by Controlling Transcriptional Pause Release from Dynamic Enhancers. Molecular cell 60, 328–337. [PubMed: 26439301]

Ganem NJ, Cornils H, Chiu SY, O'Rourke KP, Arnaud J, Yimlamai D, Thery M, Camargo FD, and Pellman D (2014). Cytokinesis failure triggers hippo tumor suppressor pathway activation. Cell 158, 833–848. [PubMed: 25126788]

Gilsbach R, Preissl S, Gruning BA, Schnick T, Burger L, Benes V, Wurch A, Bonisch U, Gunther S, Backofen R, et al. (2014). Dynamic DNA methylation orchestrates cardiomyocyte development, maturation and disease. Nature communications 5, 5288.

Gonzalez-Rosa JM, Sharpe M, Field D, Soonpaa MH, Field LJ, Burns CE, and Burns CG (2018). Myocardial Polyploidization Creates a Barrier to Heart Regeneration in Zebrafish. Developmental cell 44, 433–446.e437. [PubMed: 29486195]

Guo X, and Chen SY (2016). Dedicator of Cytokinesis 2 in Cell Signaling Regulation and Disease Development. Journal of cellular physiology.

Hagege H, Klous P, Braem C, Splinter E, Dekker J, Cathala G, de Laat W, and Forne T (2007). Quantitative analysis of chromosome conformation capture assays (3C-qPCR). Nature protocols 2, 1722–1733. [PubMed: 17641637]

Halder G, and Johnson RL (2011). Hippo signaling: growth control and beyond. Development 138, 9–22. [PubMed: 21138973]

Hansen KD, Irizarry RA, and Wu Z (2012). Removing technical variability in RNA-seq data using conditional quantile normalization. Biostatistics (Oxford, England) 13, 204–216.

Hausmann G, Banziger C, and Basler K (2007). Helping Wingless take flight: how WNT proteins are secreted. Nature reviews Molecular cell biology 8, 331–336. [PubMed: 17342185]

Heallen T, Morikawa Y, Leach J, Tao G, Willerson JT, Johnson RL, and Martin JF (2013). Hippo signaling impedes adult heart regeneration. Development 140, 4683–4690. [PubMed: 24255096]

Heinz S, Benner C, Spann N, Bertolino E, Lin YC, Laslo P, Cheng JX, Murre C, Singh H, and Glass CK (2010). Simple combinations of lineage-determining transcription factors prime cis-regulatory elements required for macrophage and B cell identities. Molecular cell 38, 576–589. [PubMed: 20513432]

Hiramoto-Yamaki N, Takeuchi S, Ueda S, Harada K, Fujimoto S, Negishi M, and Katoh H (2010). Ephexin4 and EphA2 mediate cell migration through a RhoG-dependent mechanism. The Journal of cell biology 190, 461–477. [PubMed: 20679435]

Hofsteen P, Robitaille AM, Chapman DP, Moon RT, and Murry CE (2016). Quantitative proteomics identify DAB2 as a cardiac developmental regulator that inhibits WNT/beta-catenin signaling. Proc Natl Acad Sci U S A 113, 1002–1007. [PubMed: 26755607]

Hou W, Izadi M, Nemitz S, Haag N, Kessels MM, and Qualmann B (2015). The Actin Nucleator Cobl Is Controlled by Calcium and Calmodulin. PLoS biology 13, e1002233. [PubMed: 26334624]

Jopling C, Sleep E, Raya M, Marti M, Raya A, and Izpisua Belmonte JC (2010). Zebrafish heart regeneration occurs by cardiomyocyte dedifferentiation and proliferation. Nature 464, 606–609. [PubMed: 20336145]

Kadow ZA, and Martin JF (2018). A Role for Ploidy in Heart Regeneration. Developmental cell 44, 403–404. [PubMed: 29486188]

Kalfon R, Koren L, Aviram S, Schwartz O, Hai T, and Aronheim A (2017). ATF3 expression in cardiomyocytes preserves homeostasis in the heart and controls peripheral glucose tolerance. Cardiovascular research 113, 134–146. [PubMed: 28082453]

Kokkonen-Simon KM, Saberi A, Nakamura T, Ranek MJ, Zhu G, Bedja D, Kuhn M, Halushka MK, Lee DI, and Kass DA (2018). Marked disparity of microRNA modulation by cGMP-selective PDE5 versus PDE9 inhibitors in heart disease. JCI Insight 3.

Kraut R, Chia W Fau - Jan LY, Jan Ly Fau - Jan YN, Jan Yn Fau - Knoblich JA, and Knoblich JA (1996). Role of inscuteable in orienting asymmetric cell divisions in Drosophila. Nature, 50–55. [PubMed: 8779714]

Langmead B, Trapnell C, Pop M, and Salzberg SL (2009). Ultrafast and memory-efficient alignment of short DNA sequences to the human genome. Genome biology 10, R25. [PubMed: 19261174]

Laughner JI, Ng FS, Sulkin MS, Arthur RM, and Efimov IR (2012). Processing and analysis of cardiac optical mapping data obtained with potentiometric dyes. Am J Physiol Heart Circ Physiol 303, H753–765. [PubMed: 22821993]

Leach JP, Heallen T, Zhang M, Rahmani M, Morikawa Y, Hill MC, Segura A, Willerson JT, and Martin JF (2017). Hippo pathway deficiency reverses systolic heart failure after infarction. Nature 550, 260–264. [PubMed: 28976966]

Li J, Gao E, Vite A, Yi R, Gomez L, Goossens S, van Roy F, and Radice GL (2015a). Alpha-catenins control cardiomyocyte proliferation by regulating Yap activity. Circulation research 116, 70–79. [PubMed: 25305307]

Li N, Mruk DD, Wong CK, Han D, Lee WM, and Cheng CY (2015b). Formin 1 Regulates Ectoplasmic Specialization in the Rat Testis Through Its Actin Nucleation and Bundling Activity. Endocrinology 156, 2969–2983. [PubMed: 25901598]

Lin Z, von Gise A, Zhou P, Gu F, Ma Q, Jiang J, Yau AL, Buck JN, Gouin KA, van Gorp PR, et al. (2014). Cardiac-specific YAP activation improves cardiac function and survival in an experimental murine MI model. Circulation research 115, 354–363. [PubMed: 24833660]

Love MI, Huber W, and Anders S (2014). Moderated estimation of fold change and dispersion for RNA-seq data with DESeq2. Genome biology 15, 550. [PubMed: 25516281]

Manning SA, Dent LG, Kondo S, Zhao ZW, Plachta N, and Harvey KF (2018). Dynamic Fluctuations in Subcellular Localization of the Hippo Pathway Effector Yorkie In Vivo. Current biology : CB 28, 1651–1660. [PubMed: 29754899]

Ming GL, and Song H (2005). Adult neurogenesis in the mammalian central nervous system. Annual review of neuroscience 28, 223–250.

Miyaoka Y, Ebato K, Kato H, Arakawa S, Shimizu S, and Miyajima A (2012). Hypertrophy and unconventional cell division of hepatocytes underlie liver regeneration. Current biology : CB 22, 1166–1175. [PubMed: 22658593]

Mo A, Mukamel EA, Davis FP, Luo C, Henry GL, Picard S, Urich MA, Nery JR, Sejnowski TJ, Lister R, et al. (2015). Epigenomic Signatures of Neuronal Diversity in the Mammalian Brain. Neuron 86, 1369–1384. [PubMed: 26087164]

Mohamed TMA, Ang YS, Radzinsky E, Zhou P, Huang Y, Elfenbein A, Foley A, Magnitsky S, and Srivastava D (2018). Regulation of Cell Cycle to Stimulate Adult Cardiomyocyte Proliferation and Cardiac Regeneration. Cell 173, 104–116.e112. [PubMed: 29502971]

Mootha VK, Lindgren CM, Eriksson KF, Subramanian A, Sihag S, Lehar J, Puigserver P, Carlsson E, Ridderstrale M, Laurila E, et al. (2003). PGC-1alpha-responsive genes involved in oxidative phosphorylation are coordinately downregulated in human diabetes. Nat Genet 34, 267–273. [PubMed: 12808457]

Morikawa Y, Heallen T, Leach J, Xiao Y, and Martin JF (2017). Dystrophin-glycoprotein complex sequesters Yap to inhibit cardiomyocyte proliferation. Nature 547, 227–231. [PubMed: 28581498]

Morikawa Y, Zhang M, Heallen T, Leach J, Tao G, Xiao Y, Bai Y, Willerson JT, and Martin JF (2015). Actin cytoskeletal remodeling with protrusion formation is essential for heart regeneration in Hippo deficient mice. Science signaling 8, ra41. [PubMed: 25943351]

Moroishi T, Park HW, Qin B, Chen Q, Meng Z, Plouffe SW, Taniguchi K, Yu FX, Karin M, Pan D, et al. (2015). A YAP/TAZ-induced feedback mechanism regulates Hippo pathway homeostasis. Genes & development 29, 1271–1284. [PubMed: 26109050]

Naya FJ, Black BL, Wu H, Bassel-Duby R, Richardson JA, Hill JA, and Olson EN (2002). Mitochondrial deficiency and cardiac sudden death in mice lacking the MEF2A transcription factor. Nature medicine 8, 1303–1309.

Nomura S, Satoh M, Fujita T, Higo T, Sumida T, Ko T, Yamaguchi T, Tobita T, Naito AT, Ito M, et al. (2018). Cardiomyocyte gene programs encoding morphological and functional signatures in cardiac hypertrophy and failure. Nature communications 9, 4435.

Nomura S, Satoh M, Fujita T, Higo T, Sumida T.A.-O.h.o.o., Ko T, Yamaguchi T, Tobita T, Naito AT, Ito M, et al. Cardiomyocyte gene programs encoding morphological and functional signatures in cardiac hypertrophy and failure.

Nord AS, Blow MJ, Attanasio C, Akiyama JA, Holt A, Hosseini R, Phouanenavong S, Plajzer-Frick I, Shoukry M, Afzal V, et al. (2013). Rapid and pervasive changes in genome-wide enhancer usage during mammalian development. Cell 155, 1521–1531. [PubMed: 24360275]

Pachori AS, Custer L, Hansen D, Clapp S, Kemppa E, and Klingensmith J (2010). Bone morphogenetic protein 4 mediates myocardial ischemic injury through JNK-dependent signaling pathway. Journal of molecular and cellular cardiology 48, 1255–1265. [PubMed: 20096288]

Park GS, Oh H, Kim M, Kim T, Johnson RL, Irvine KD, and Lim DS (2016). An evolutionarily conserved negative feedback mechanism in the Hippo pathway reflects functional difference between LATS1 and LATS2. Oncotarget 7, 24063–24075. [PubMed: 27006470]

Passer D, van de Vrugt A, Atmanli A, and Domian IJ (2016). Atypical Protein Kinase C-Dependent Polarized Cell Division Is Required for Myocardial Trabeculation. Cell reports 14, 1662–1672. [PubMed: 26876178]

Patterson M, Barske L, Van Handel B, Rau CD, Gan P, Sharma A, Parikh S, Denholtz M, Huang Y, Yamaguchi Y, et al. (2017). Frequency of mononuclear diploid cardiomyocytes underlies natural variation in heart regeneration. Nat Genet 49, 1346–1353. [PubMed: 28783163]

Piccolo S, Dupont S, and Cordenonsi M (2014). The biology of YAP/TAZ: hippo signaling and beyond. Physiological reviews 94, 1287–1312. [PubMed: 25287865]

Preissl S, Schwaderer M, Raulf A, Hesse M, Gruning BA, Kobele C, Backofen R, Fleischmann BK, Hein L, and Gilsbach R (2015). Deciphering the Epigenetic Code of Cardiac Myocyte Transcription. Circulation research 117, 413–423. [PubMed: 26105955]

Puente BN, Kimura W, Muralidhar SA, Moon J, Amatruda JF, Phelps KL, Grinsfelder D, Rothermel BA, Chen R, Garcia JA, et al. (2014). The oxygen-rich postnatal environment induces cardiomyocyte cell-cycle arrest through DNA damage response. Cell 157, 565–579. [PubMed: 24766806]

Pugach EK, Richmond PA, Azofeifa JG, Dowell RD, and Leinwand LA (2015). Prolonged Cre expression driven by the alpha-myosin heavy chain promoter can be cardiotoxic. Journal of molecular and cellular cardiology 86, 54–61. [PubMed: 26141530]

Quinlan AR (2014). BEDTools: The Swiss-Army Tool for Genome Feature Analysis. Current protocols in bioinformatics 47, 11.12.11–34.

Ragni CV, Diguet N, Le Garrec JF, Novotova M, Resende TP, Pop S, Charon N, Guillemot L, Kitasato L, Badouel C, et al. (2017). Amotl1 mediates sequestration of the Hippo effector Yap1 downstream of Fat4 to restrict heart growth. Nature communications 8, 14582.

Ramirez F, Ryan DP, Gruning B, Bhardwaj V, Kilpert F, Richter AS, Heyne S, Dundar F, and Manke T (2016). deepTools2: a next generation web server for deep-sequencing data analysis. Nucleic acids research 44, W160–165. [PubMed: 27079975]

Reynolds JO, Quick AP, Wang Q, Beavers DL, Philippen LE, Showell J, Barreto-Torres G, Thuerauf DJ, Doroudgar S, Glembotski CC, et al. (2016). Junctophilin-2 gene therapy rescues heart failure by normalizing RyR2-mediated Ca(2+) release. Int J Cardiol 225, 371–380. [PubMed: 27760414]

Richardson GD (2016). Simultaneous Assessment of Cardiomyocyte DNA Synthesis and Ploidy: A Method to Assist Quantification of Cardiomyocyte Regeneration and Turnover. Journal of visualized experiments : JoVE.

Saarikangas J, Mattila PK, Varjosalo M, Bovellan M, Hakanen J, Calzada-Wack J, Tost M, Jennen L, Rathkolb B, Hans W, et al. (2011). Missing-in-metastasis MIM/MTSS1 promotes actin assembly at intercellular junctions and is required for integrity of kidney epithelia. Journal of cell science 124, 1245–1255. [PubMed: 21406566]

Sawicka A, and Seiser C (2012). Histone H3 phosphorylation - a versatile chromatin modification for different occasions. Biochimie 94, 2193–2201. [PubMed: 22564826]

Schep AN, Buenrostro JD, Denny SK, Schwartz K, Sherlock G, and Greenleaf WJ (2015). Structured nucleosome fingerprints enable high-resolution mapping of chromatin architecture within regulatory regions. Genome research 25, 1757–1770. [PubMed: 26314830]

Sohal DS, Nghiem M, Crackower MA, Witt SA, Kimball TR, Tymitz KM, Penninger JM, and Molkentin JD (2001). Temporally regulated and tissue-specific gene manipulations in the adult and embryonic heart using a tamoxifen-inducible Cre protein. Circulation research 89, 20–25. [PubMed: 11440973]

Soonpaa MH, and Field LJ (1997). Assessment of cardiomyocyte DNA synthesis in normal and injured adult mouse hearts. The American journal of physiology 272, H220–226. [PubMed: 9038941]

Sorrells SF, Paredes MF, Cebrian-Silla A, Sandoval K, Qi D, Kelley KW, James D, Mayer S, Chang J, Auguste KI, et al. (2018). Human hippocampal neurogenesis drops sharply in children to undetectable levels in adults. Nature 555, 377–381. [PubMed: 29513649]

Stein C, Bardet AF, Roma G, Bergling S, Clay I, Ruchti A, Agarinis C, Schmelzle T, Bouwmeester T, Schubeler D, et al. (2015). YAP1 Exerts Its Transcriptional Control via TEAD-Mediated Activation of Enhancers. PLoS genetics 11, e1005465. [PubMed: 26295846]

Stergachis AB, Neph S, Reynolds A, Humbert R, Miller B, Paige SL, Vernot B, Cheng JB, Thurman RE, Sandstrom R, et al. (2013). Developmental fate and cellular maturity encoded in human regulatory DNA landscapes. Cell 154, 888–903. [PubMed: 23953118]

Subramanian A, Tamayo P, Mootha VK, Mukherjee S, Ebert BL, Gillette MA, Paulovich A, Pomeroy SL, Golub TR, Lander ES, et al. (2005). Gene set enrichment analysis: a knowledge-based approach for interpreting genome-wide expression profiles. Proc Natl Acad Sci U S A 102, 15545–15550. [PubMed: 16199517]

Tripathi S, Pohl MO, Zhou Y, Rodriguez-Frandsen A, Wang G, Stein DA, Moulton HM, DeJesus P, Che J, Mulder LC, et al. (2015). Meta- and Orthogonal Integration of Influenza "OMICs" Data Defines a Role for UBR4 in Virus Budding. Cell host & microbe 18, 723–735. [PubMed: 26651948]

Tzahor E (2007). Wnt/beta-catenin signaling and cardiogenesis: timing does matter. Developmental cell 13, 10–13. [PubMed: 17609106]

Tzahor E, and Poss KD (2017). Cardiac regeneration strategies: Staying young at heart. Science (New York, NY) 356, 1035–1039.

Uosaki H, Cahan P, Lee DI, Wang S, Miyamoto M, Fernandez L, Kass DA, and Kwon C (2015). Transcriptional Landscape of Cardiomyocyte Maturation. Cell reports 13, 1705–1716. [PubMed: 26586429]

van de Werken HJ, de Vree PJ, Splinter E, Holwerda SJ, Klous P, de Wit E, and de Laat W (2012). 4C technology: protocols and data analysis. Methods in enzymology 513, 89–112. [PubMed: 22929766]

Vinnakota KC, and Bassingthwaighte JB (2004). Myocardial density and composition: a basis for calculating intracellular metabolite concentrations. Am J Physiol Heart Circ Physiol 286, H1742–1749. [PubMed: 14693681]

Vujic A, Lerchenmuller C, Wu TD, Guillermier C, Rabolli CP, Gonzalez E, Senyo SE, Liu X, Guerquin-Kern JL, Steinhauser ML, et al. (2018). Exercise induces new cardiomyocyte generation in the adult mammalian heart. Nature communications 9, 1659.

Walter W, Sanchez-Cabo F, and Ricote M (2015). GOplot: an R package for visually combining expression data with functional analysis. Bioinformatics (Oxford, England) 31, 2912–2914.

Wang J, Bai Y, Li N, Ye W, Zhang M, Greene SB, Tao Y, Chen Y, Wehrens XH, and Martin JF (2014). Pitx2-microRNA pathway that delimits sinoatrial node development and inhibits predisposition to atrial fibrillation. Proc Natl Acad Sci U S A 111, 9181–9186. [PubMed: 24927531]

Wang J, Greene SB, and Martin JF (2011). BMP signaling in congenital heart disease: new developments and future directions. Birth defects research Part A, Clinical and molecular teratology 91, 441–448. [PubMed: 21384533]

Wang J, and Martin JF (2014). Macro advances in microRNAs and myocardial regeneration. Current opinion in cardiology 29, 207–213. [PubMed: 24625819]

Willis MS, Schisler JC, Portbury AL, and Patterson C (2009). Build it up-Tear it down: protein quality control in the cardiac sarcomere. Cardiovascular research 81, 439–448. [PubMed: 18974044]

Xin M, Olson EN, and Bassel-Duby R (2013). Mending broken hearts: cardiac development as a basis for adult heart regeneration and repair. Nature reviews Molecular cell biology 14, 529–541. [PubMed: 23839576]

Zanconato F, Forcato M, Battilana G, Azzolin L, Quaranta E, Bodega B, Rosato A, Bicciato S, Cordenonsi M, and Piccolo S (2015). Genome-wide association between YAP/TAZ/TEAD and AP-1 at enhancers drives oncogenic growth. Nature cell biology 17, 1218–1227. [PubMed: 26258633]

Zhao B, Li L, Tumaneng K, Wang CY, and Guan KL (2010). A coordinated phosphorylation by Lats and CK1 regulates YAP stability through SCF(beta-TRCP). Genes & development 24, 72–85. [PubMed: 20048001]

Zhao B, Wei X, Li W, Udan RS, Yang Q, Kim J, Xie J, Ikenoue T, Yu J, Li L, et al. (2007). Inactivation of YAP oncoprotein by the Hippo pathway is involved in cell contact inhibition and tissue growth control. Genes & development 21, 2747–2761. [PubMed: 17974916]

Zhao C, Guo H, Li J, Myint T, Pittman W, Yang L, Zhong W, Schwartz RJ, Schwarz JJ, Singer HA, et al. (2014). Numb family proteins are essential for cardiac morphogenesis and progenitor differentiation. Development 141, 281–295. [PubMed: 24335256]

Zhu J, Adli M, Zou JY, Verstappen G, Coyne M, Zhang X, Durham T, Miri M, Deshpande V, De Jager PL, et al. (2013). Genome-wide chromatin state transitions associated with developmental and environmental cues. Cell 152, 642–654. [PubMed: 23333102]

Highlights

- Creation of a mouse conditionally expressing active YAP, called YAP5SA
- YAP5SA in adult cardiomyocytes (CMs) induces more primitive transcriptional state
- YAP5SA reveals developmental enhancers and suppresses adult enhancers
- YAP5SA expression in CMs causes CM hyperplasia and overall heart hypercellularity

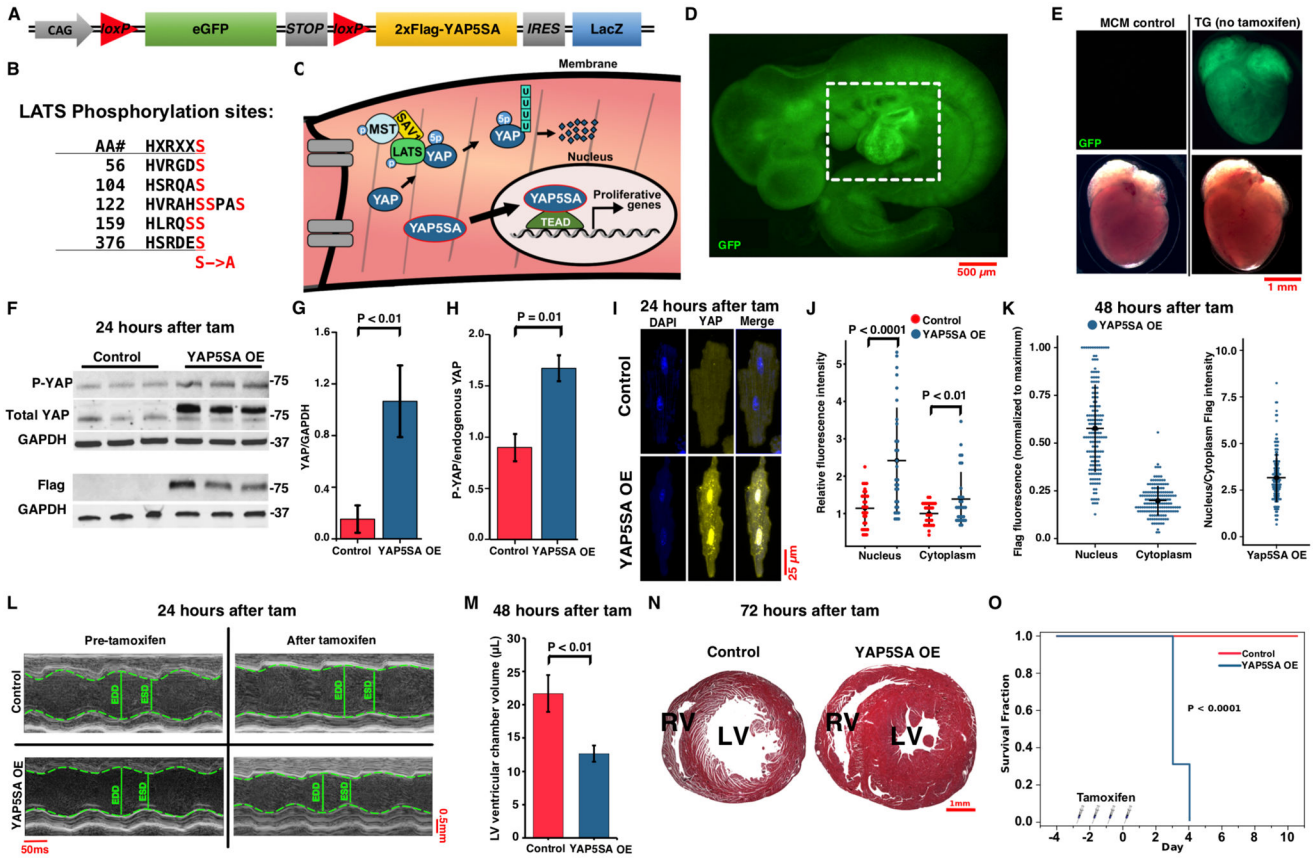

Figure 1. Design and expression of YAP5SA transgene.

(A) YAP5SA transgene (TG). **(B)** Serine phosphorylation sites mutated in YAP5SA (STAR methods). **(C)** Model of Hippo signaling in adult CMs. **(D)** E9.5 YAP5SA with GFP expression. **(E)** GFP fluorescence in MCM and TG hearts at P0. **(F)** Western blot: Flag-YAP5SA and phosphorylation of endogenous YAP 24 hrs after fourth tam. Controls: MCM mice with tam. **(G, H)** Western blot quantification. Total YAP & Flag n=3 mice/genotype. P-YAP (mouse S112) control n=4, YAP5SA n=3. **(I)** IF of control and YAP5SA OE CMs 24 hrs after fourth tam. **(J)** Quantification of nuclear and cytoplasmic YAP IF in CMs from control or YAP5SA OE, shown as dot plots with mean +/− SDM, relative to mean control cytoplasmic intensity. Control n=3 hearts, 30 CMs. YAP5SA OE n=3 hearts, 30 CMs. Control: MCM with tam. **(K)** Quantification of Flag IF in YAP5SA OE CMs, shown as dot plots with mean +/− SDM. n=3 hearts, 50 CMs each, 48 hrs after tam. **(L)** M-mode ECHO before and 24 hrs after tam. Control: MCM mice with tam. **(M)** LV chamber volume control and YAP5SA OE 48 hrs after tam. n=6/group. Control: MCM mice with tam. **(N)** Histology 72 hrs after tam. Control: MCM with tam. **(O)** Kaplan Meier survival analysis control (n=11) and YAP5SA OE (n=13). Statistics: Mantel-Cox test. Control: MCM with tam. G,H,J,M groups compared by ANOVA with Bonferroni post-hoc tests. G,H,M shown as Mean +/− SEM. See also Fig. S1 and S2.

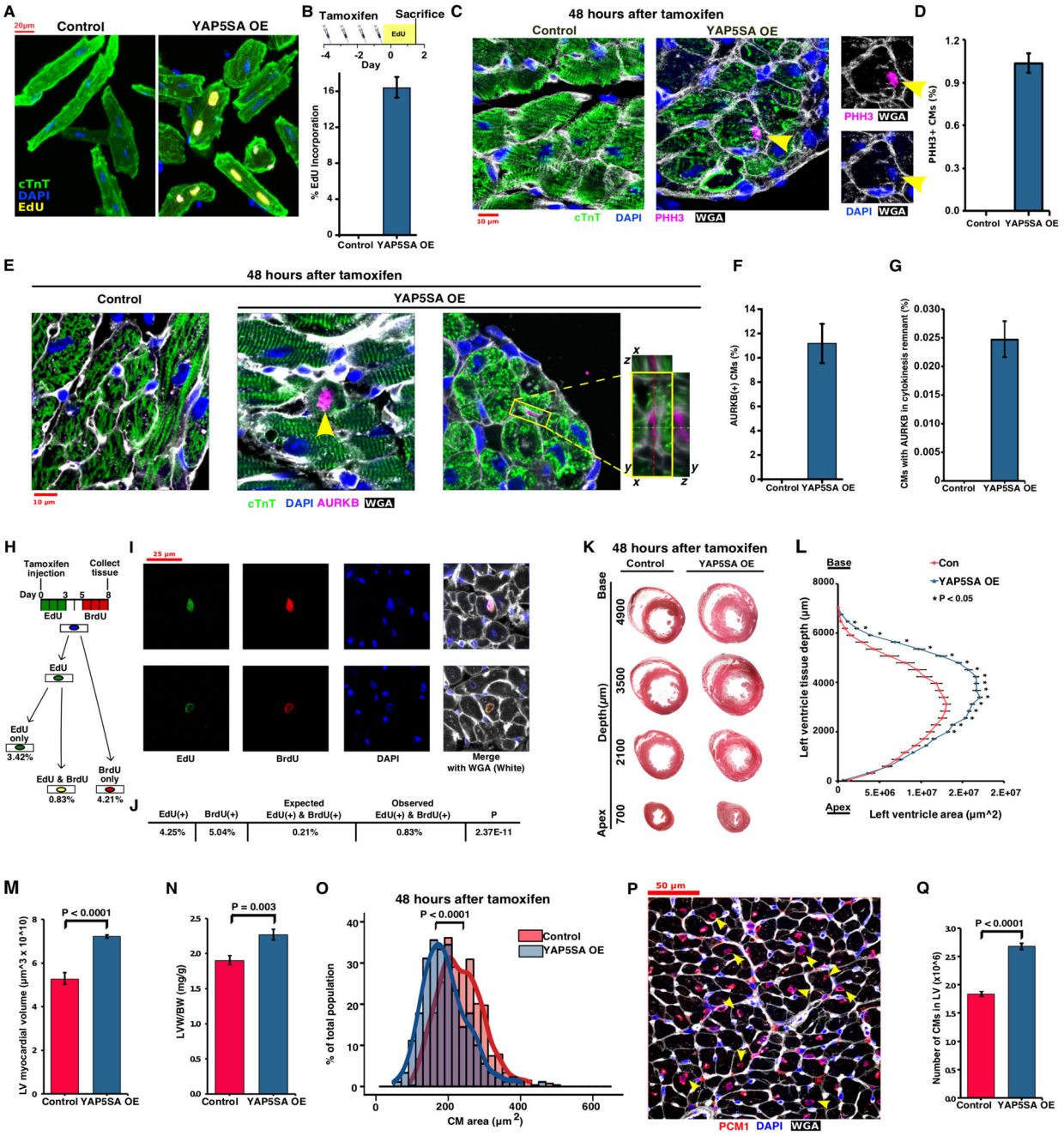

Figure 2. Proliferation of adult cardiomyocytes.

(A) EdU-stained CMs. **(B)** tam & EdU labeling strategy; Quantification of EdU incorporation (n=4 hearts/group, 200-300 CMs/heart). **(C)** pHH3 IF Control: MCM with tam. Positive CM indicated (yellow arrow) separate channels on right **(D)** pHH3 quantification in CMs. YAP5SA n=5; Controls n=9; 3 MCM with & 3 no tam, and 3 YAP5SA MCM mice no tam. 300-400 CMs/heart, 48 hrs after fourth tam injection. **(E)** AURKB IF: Positive CMs indicated (yellow arrows) or inset with z-projection. Control: MCM with tam. **(F)** Quantification of AURKB(+) CM nuclei (n=3 YAP5SA; Control n=9 mice; 3 MCM with & 3 no tam, and 3 YAP5SA MCM mice no tam. 200-300 CMs/heart, 48

hrs after fourth tam). **(G)** Quantification of AURKB in cytokinesis remnant (YAP5SA n=3; Control n=9, 3 MCM with & 3 no tam, and 3 YAP5SA MCM no tam. 48 hrs after fourth tam ~30mm^2 imaged each with ~900 CMs/mm^3). **(H)** EdU & BrdU labeling protocol and % of labeled CMs from low dose protocol. **(I)** EdU(+) and BrdU(+) CMs with WGA. **(J)** Chi-squared table of labeled CMs. **(K)** Sections of LV at indicated depth **(L)** Area of LV at indicated depth * $P<0.05$ significance **(M)** Total LV tissue volume **(N)** Ratio of LV weight/body weight (K-N n=6 YAP5SA; Controls n=12, 3 YAP5SA MCM no tam, 3 MCM no tam, 6 MCM with tam), 48 hrs after fourth tam **(O)** Histograms of areas of isolated CMs from control and YAP5SA. YAP5SA n=6; Controls n=9, 3 YAP5SA MCM no tam, 3 MCM no tam, 3 MCM with tam; ~100 cells/heart, 48 hrs after fourth tam. **(P)** CMs labeled with PCM-1 (Yellow arrows). **(Q)** CM number in LV (YAP5SA n=5; Control n=11, 5 MCM with tam, 3 YAP5SA no tam, 3 MCM no tam), 48 hrs after fourth tam. L-O,Q groups compared by ANOVA with post-hoc Bonferroni tests; and tam protocol from 2B. Data in B,D,F,G,L,M,N,Q shown as mean +/−SEM. See also Fig. S1.

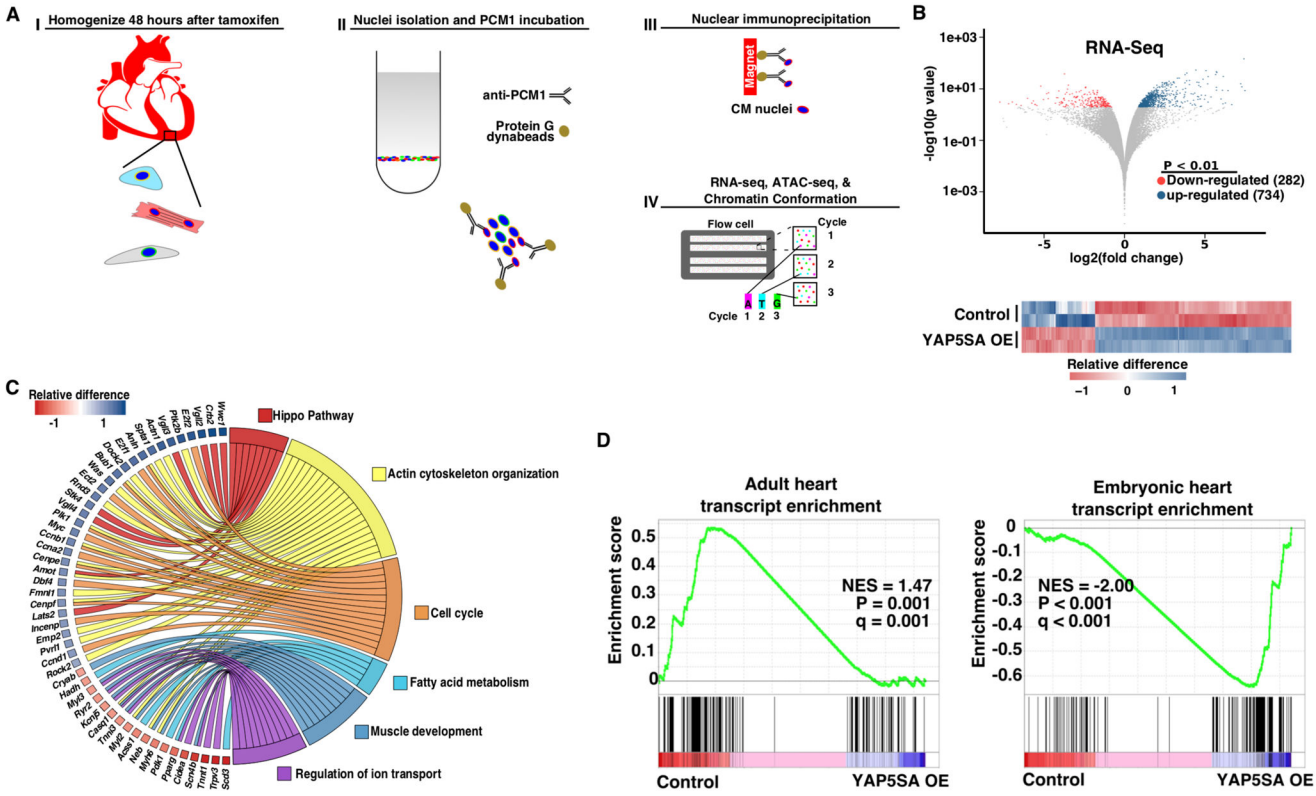

Figure 3. YAP5SA cardiomyocytes express a primitive genetic profile.

(A) Protocol for CM-enriched nuclear RNA and ATAC-seq. Control: MCM with tam. 48 hrs after tam. **(B)** (Top) Volcano plot of YAP5SA RNA-seq adjusted P-value<0.01, 734 genes up-regulated; 282 down-regulated. Two samples/genotype. (Bottom) Heat map differentially regulated genes. **(C)** Circle plot of select genes indicated ontologies. Gene expression relative difference (log2 fold change). (**D)** Gene set enrichment analysis of top 200 most differentially regulated genes: adult hearts relative to embryonic (left) or embryonic relative to adult (right) against RNA-seq dataset (normalized enrichment score, NES, relative to control. Data from (Uosaki et al.,2015). See Fig. S2,S3 and S4.

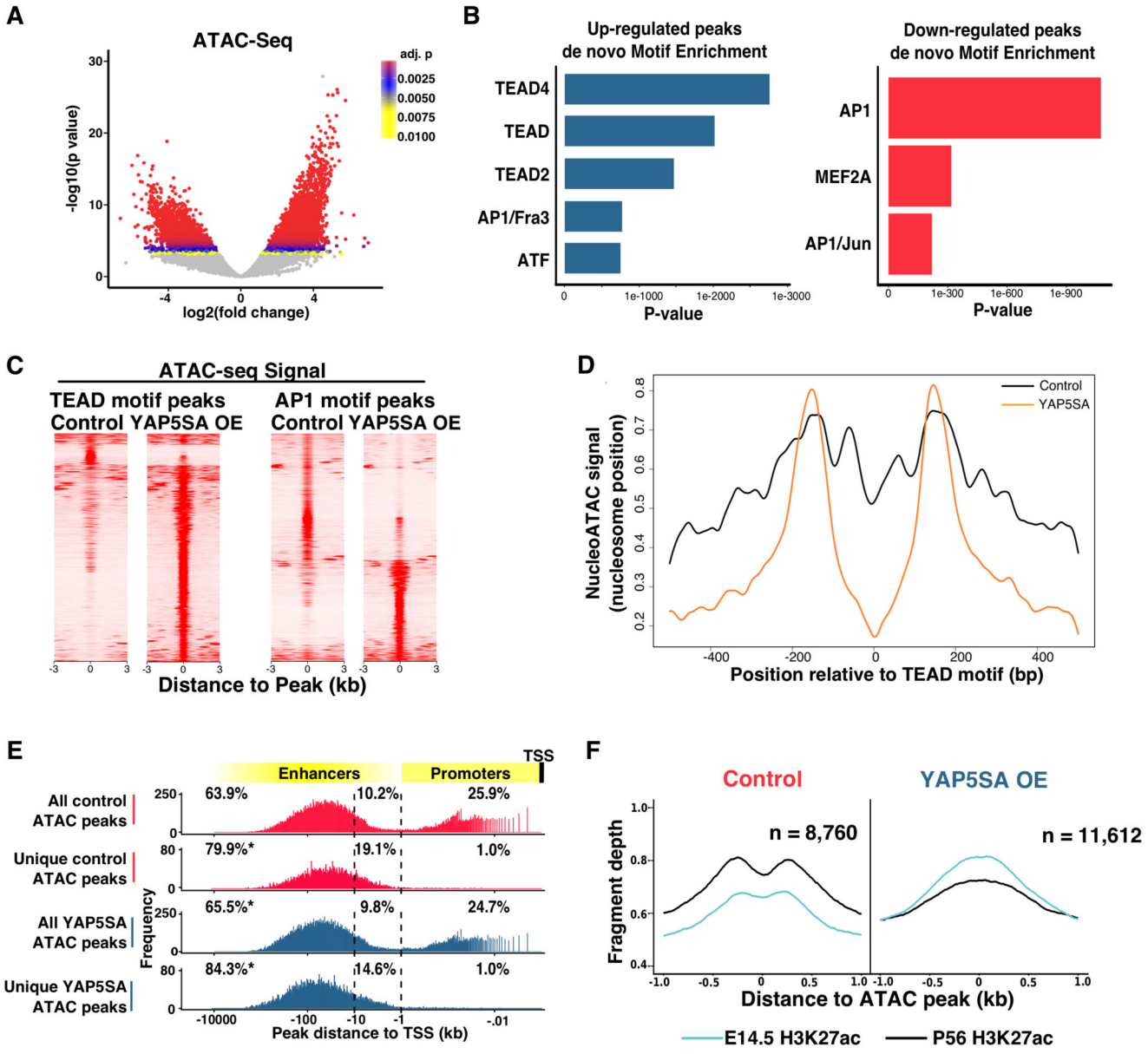

Figure 4. YAP5SA opens chromatin at TEAD and AP-1 elements

(A) Volcano plot of YAP5SA ATAC-seq. YAP5SA OE CMs: 11,612 peaks up-regulated and 8,760 down-regulated at P<0.035 log2 fold change. Two samples/genotype. **(B)** (Left) Enriched motifs in ATAC-seq peaks from YAP5SA OE CMs. (Right) Enriched motifs in ATAC-seq peaks from control CMs (adjusted P<0.035). **(C)** ATAC-seq signal at all peaks containing TEAD (left) or AP-1 (right) motifs. **(D)** Nucleosome signal for all TEAD motif peaks, normalized between 0 and 1. **(E)** Distance to TSS of ATAC-seq peaks. * P≤0.001 relative to control ATAC proportions. (Chisquared test with Yates correction). **(F)** H3K27Ac fragment coverage from E14.5 and P56 hearts centered around top ATAC-seq peaks (adjusted P≤0.035). N: number of interrogated ATAC-seq peaks. See also Fig. S3 and S4.

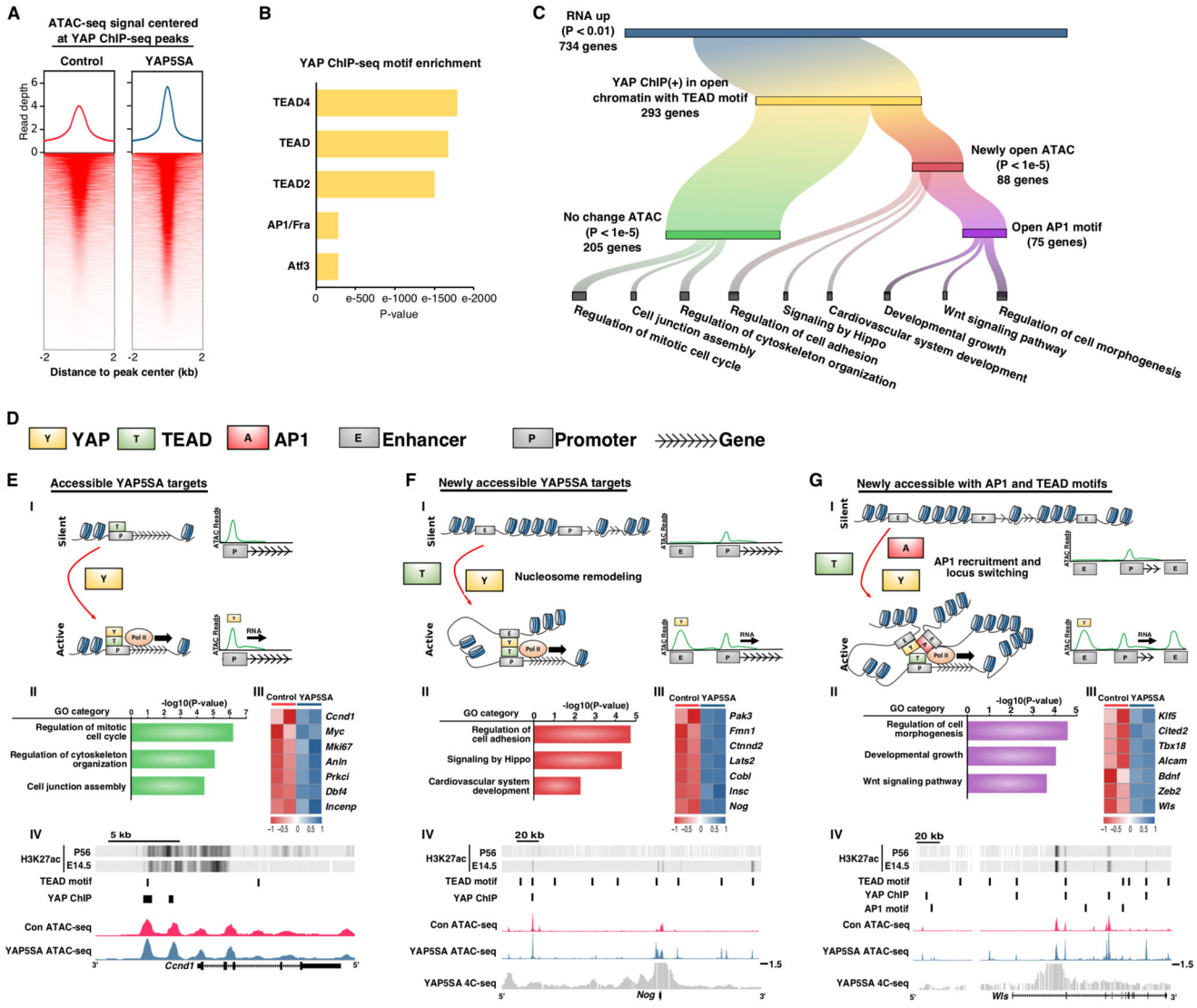

Figure 5. Identification of YAP targets and YAP5SA mechanism

(A) Heat map of ATAC-seq reads centered at YAP ChIP-seq peaks. **(B)** Enriched transcription factor motifs in YAP ChIP-seq peaks (GSM2220157) **(C)** YAP5SA target genes and gene ontologies from integrated genomics (RNA-seq up P<0.01; YAP ChIP-seq peak in open chromatin [normalized read count < 2 over the peak] & containing a TEAD motif; ATAC-seq up [$P < 1e^{-5}$]). **(D)** Model key **(E)** I. Model of YAP5SA activation by binding to promoters of already accessible genes: RNA up, ATAC no change, open TEAD motifs. II. Gene ontology of 205 genes fitting this criteria; and III. Heat map of selected genes. IV. Sequencing track. **(F)** I. Model of YAP5SA activation of genes through chromatin remodeling: RNA up, ATAC up, newly open TEAD motifs. II. Gene ontology of 88 genes fitting this criteria; and III. Heat map of selected genes. IV. Sequencing track. **(G)** I. Model of YAP5SA Activation of genes with AP-1-asociated open chromatin: RNA up, ATAC up, open, newly open TEAD motifs & AP-1 motifs. II. Gene ontology of 75 genes fitting this criteria; and III. Heat map of selected genes. IV. Sequencing track. AIV, BIV, and CIV are

density plots indicating reads from H3K27ac ChIP-seq data from adult and embryonic hearts and our 4C data. TEAD motifs and AP-1 motifs indicated. 5’ and 3’ are shown relative to top strand of DNA. For E-G See Table S1. full gene lists. ATAC-seq tracks scaled to YAP5SA OE maximum. Black notch scale on the 4C-seq tracks indicates 4C coverage/$1e^3$ reads.

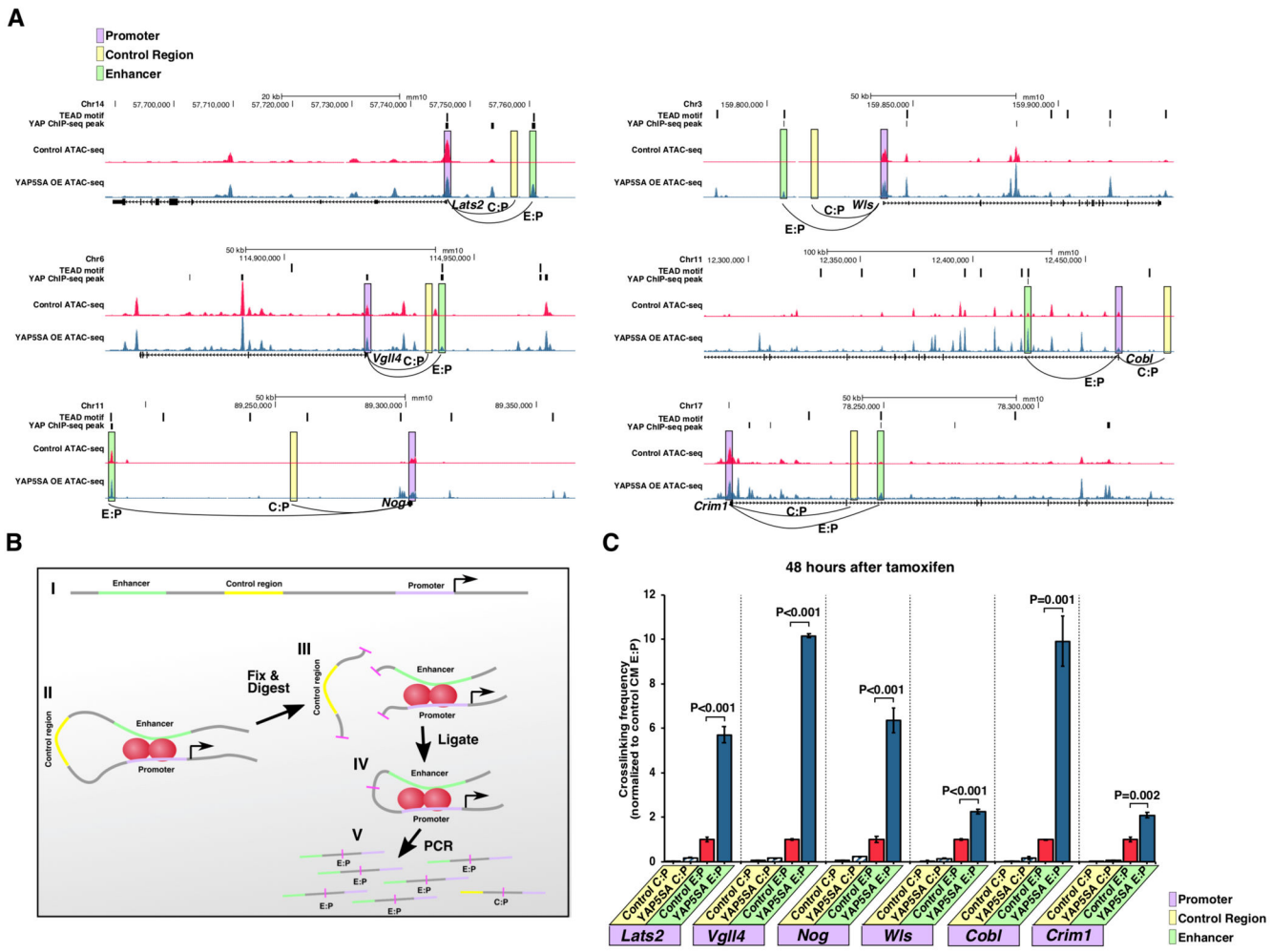

Figure 6. YAP5SA increases enhancer-promoter contacts

(A) Gene tracks with enhancers (green). Control regions closer to promoter than enhancer used for 3C (yellow). Promoters (purple). C:P, Control to Promoter contact. E:P, Enhancer to Promoter contact. **(B)** Cartoon of difference between 2D and 3D enhancer-promoter proximity. (I) 2D proximity. (II) 3D proximity (III) fixing DNA/chromatin interactions and digesting DNA. Loci not in contact diffuse away. (IV) Ligation of loci in contact. (V) qPCR of ligated loci. E:P interactions are more common than C:P, reflecting contact frequency **(C)** Quantification of chromatin contact in CM nuclei by 3C at genomic loci indicated in Fig. 7A, normalized to Control CM enhancer-promoter contacts. Groups compared: ANOVA with post-hoc Bonferroni tests. Data shown mean +/− SEM. n=3 replicates/group (from pooled CM nuclei from 6 Control hearts or 6 YAP5SA OE hearts, STAR methods). Controls: both YAP5SA no tam and tam-injected MCM control. See Table S2 for primers.

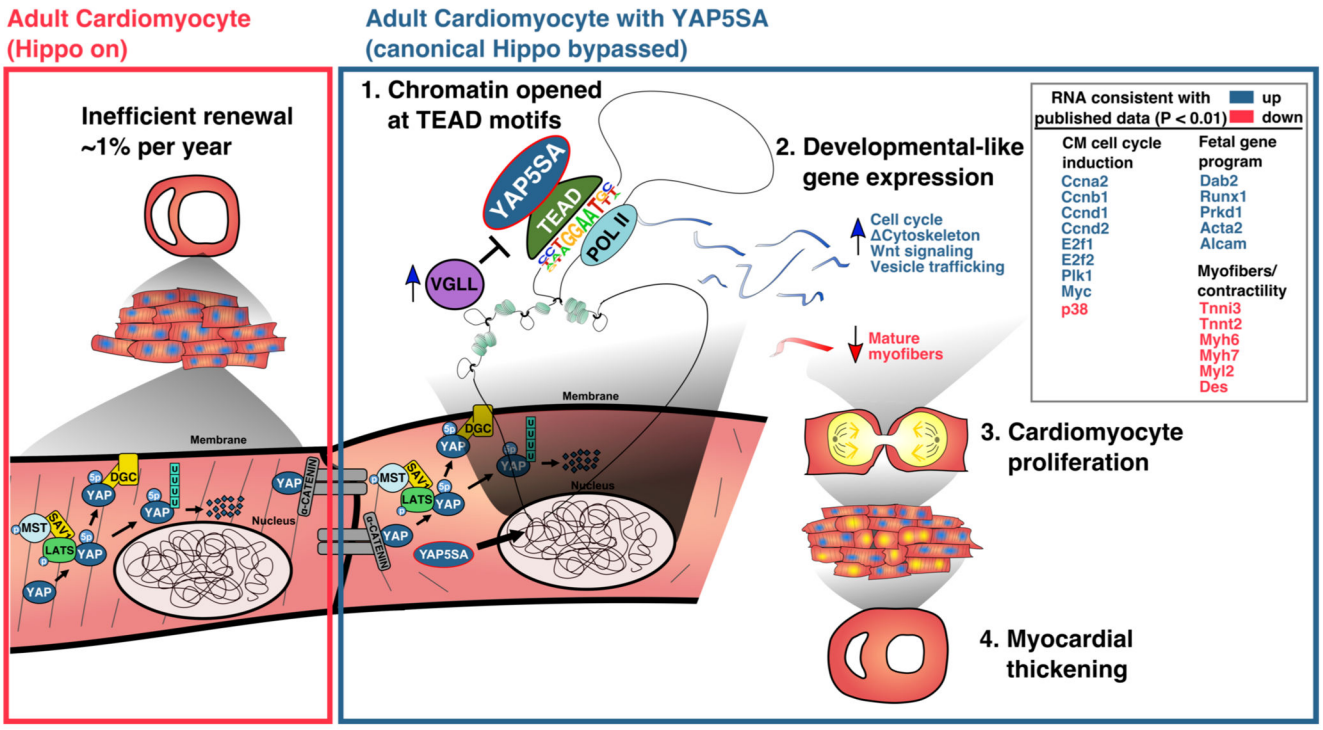

Figure 7. Model.

Adult CMs have high Hippo activity. YAP5SA bypasses canonical Hippo inhibition: (1) chromatin remodeling centered around TEAD motifs. (2) gene expression resembling fetal CMs – expression of cell-cycle genes and reduced expression of cytoskeletal and contractile genes. Previously published observations indicated. (3) CM proliferation. (4) Thickening of myocardium. Vestigial-like genes are up-regulated and antagonize YAP-dependent de-differentiation.

KEY RESOURCES TABLE

REAGENT or RESOURCE	SOURCE	IDENTIFIER
Antibodies		
Phospho-YAP(Ser127) antibody	Cell signaling technology	Cat#4911
Rabbit YAP1 antibody	Novus biologicals	Cat#NB110-583538
Donkey anti-Rabbit, Alexa 488	Thermo Fisher Scientific	Cat#A-21206
Donkey anti-Rabbit, Alexa 647	Thermo Fisher Scientific	Cat#A-31573
Donkey anti-Rabbit, Alexa 546	Thermo Fisher Scientific	Cat#A-10040
Donkey anti-Mouse, Alexa 488	Thermo Fisher Scientific	Cat#A-21202
Donkey anti-Mouse, Alexa 546	Thermo Fisher Scientific	Cat#A-10036
Donkey anti-chicken, Alexa 488	Thermo Fisher Scientific	Cat#A-11039
Donkey anti-rat, Alexa 488	Thermo Fisher Scientific	Cat#A-11006
IRDye® 800CW Goat anti-Mouse IgG	LI-COR	Cat#925-32210
IRDye® 680RD Goat anti-Rabbit IgG	LI-COR	Cat#925-68071
Mouse anti-cTnT	Thermo Fisher Scientific	Cat#MA5-12960
Mouse anti-cTnT-Alexa 647 conjugate	BD Pharmingen	cat#565744
Mouse anti-AuroraKB	Novus	Cat#NBP2-50039
Rat anti-PHH3	Abcam	Cat#ab10543
Mouse anti-M2Flag	Sigma-Aldrich	Cat#F1804
Mouse anti-GAPDH	Millipore	Cat#CB1001
Rabbit Anti-PCM-1	Sigma-Aldrich	Cat#HPA023370
Chicken anti-β-gal	Abcam	Cat#ab9361
Rabbit anti-N-cadherin	Abcam	Cat#ab76057
Rat anti-BrdU	Accurate Chemical & Scientific corp	Cat#OBT0030
Rabbit DYKDDDDK Tag Antibody	Cell signaling technology	Cat#2368
Bacterial and Virus Strains		
pCMV-flag YAP25SA	Addgene, Kun-Liang Guan	plasmid # 27371
Chemicals, Peptides, and Recombinant Proteins		
Tamoxifen	Sigma-Aldrich	Cat#T5648
Collagenase A	Sigma-Aldrich	Cat#10103586001
Blebbistatin	Sigma-Aldrich	Cat#B0560
di-4-ANEPS	Invitrogen	Cat#D-1199
BglII	NEB	Cat#R0143S
EcoRI-HF®	NEB	Cat#R3101
BsrGI-HF®	NEB	Cat#R3575L
T4 DNA ligase (3C)	NEB	Cat#R3575L
Proteinase K	Sigma-Aldrich	Cat#P2308-25MG
RNAse A	Sigma-Aldrich	Cat#10109142001
Protein-G Dynabeads	ThermoFisher Scientific	Cat#10004D

REAGENT or RESOURCE	SOURCE	IDENTIFIER
Rhodamine conjugated WGA	Vector Labs	Cat#RL-1022
DAPI	Thermo Fisher Scientific	Cat#62248
OptiPrem Density Gradient Medium	Sigma-Aldrich	Cat#D1556
Critical Commercial Assays		
Click-iT EdU Alexa Fluor 647 Imaging Kit	ThermoFisher Scientific	Cat#C10340
iTaq™ Universal SYBR® Green Supermix	Bio-Rad	Cat#1725120
DpnII	NEB	Cat#R0543M
T4 DNA ligase (4C)	Roche	Cat#10799009001
Proteinase K (4C)	Thermo Fisher	Cat#EO0491
NucleoMag 96 PCR kit	Macherey-Nagel	Cat#744100.1
Csp6I	Thermo Fisher	Cat#ER0211
Expand Long template polymerase	Roche	Cat#11681842001
Agencourt AMPure XP beads	Beckman Coulter	Cat#A63881
Tissue-Tek® O.C.T. Compound, Sakura® Finetek	V.W.R.	Cat#25608-930
Deposited Data		
H3K27ac ChIP-seq E14.5 heart	Gene Expression Omnibus	GSM1264374
H3K27ac ChIP-seq E14.5 heart	Gene Expression Omnibus	GSM1264384
Sham 1 (mRNA-seq)	Gene Expression Omnibus	GSM3056373
Sham 2 (mRNA-seq)	Gene Expression Omnibus	GSM3056374
Sham 3 (mRNA-seq)	Gene Expression Omnibus	GSM3056375
Sham 4 (mRNA-seq)	Gene Expression Omnibus	GSM3056376
Sham 5 (mRNA-seq)	Gene Expression Omnibus	GSM3056377
Sham 5 (mRNA-seq)	Gene Expression Omnibus	GSM3056378
TAC 2 (mRNA-seq)	Gene Expression Omnibus	GSM3056379
TAC 3 (mRNA-seq)	Gene Expression Omnibus	GSM3056380
TAC 4 (mRNA-seq)	Gene Expression Omnibus	GSM3056381
TAC 5 (mRNA-seq)	Gene Expression Omnibus	GSM3056382
H3K27ac ChIP-seq TAC operation (Week 1)	Gene Expression Omnibus	GSM2497652
H3K27ac ChIP-seq TAC operation (Week 8)	Gene Expression Omnibus	GSM2687477
YAP ChIP-seq	Gene Expression Omnibus	GSM2220157
Our YAP5SA OE ATAC-seq	This paper, Gene Expression Omnibus	GSE123457
Our Control ATAC-Seq	This paper, Gene Expression Omnibus	GSE123457
Our YAP5SA OE RNA-seq	This paper, Gene Expression Omnibus	GSE123457
Our Control RNA-Seq	This paper, Gene Expression Omnibus	GSE123457

REAGENT or RESOURCE	SOURCE	IDENTIFIER
Our 4C-seq	This paper, Gene Expression Omnibus	GSE123457
Embryonic and adult mRNA data	Kwon, et al.	
Experimental Models: Organisms/Strains		
αMyHC-Cre-ERT2 mice	Sohal et al.	
Tg(Jojo_Flag::YAP5SA)5JFM mice	This paper	
Oligonucleotides		
Genotyping primers	See Table S2	
4C primers	See Table S2	
3C primers	See Table S2	
Software and Algorithms		
FIJI	National Institutes of Health	https://fiji.sc/
R	R Core Team	https://www.r-project.org/
GraphPad Prism 5	GraphPad Software, Inc	https://www.graphpad.com/scientific-software/prism/
Inkscape	Nathan Hurst	https://inkscape.org/en/
Metascape	Tripathi et al.	http://metascape.org
GOPlot	Walter, et al.	http://wencke.github.io
GSEA	Broad Institute, Inc.	http://software.broadinstitute.org/gsea/index.jsp
Bowtie2	Ferragina, et al.	http://bowtie-bio.sourceforge.net/bowtie2/index.shtml
Picard-MarkDuplicates	Broad Institute, Inc.	https://broadinstitute.github.io/picard/
MACS2	Zhang et al.	http://liulab.dfci.harvard.edu/MACS/
Bedtools	Quinlan laboratory, University of Utah	https://bedtools.readthedocs.io/en/latest/content/bedtools-suite.html
CQN	Hansen, et al.	http://bioconductor.org/packages/release/bioc/html/cqn.html
DESeq2	Love, et al.	https://bioconductor.org/packages/release/bioc/html/DESeq2.html
NucleoATAC	Schep, et al.	https://nucleoatac.readthedocs.io/en/latest/
HOMER oftware for motif discovery and next generation sequencing analysis	Heinz et al.	http://homer.ucsd.edu/homer/index.html
deepTools	Ramírez, et al.	https://deeptools.readthedocs.io/en/develop/
UCSC genome browser	University of California, Santa Cruz	https://genome.ucsc.edu
liftOver	University of California, Santa Cruz	https://genome.ucsc.edu/cgi-bin/hgLiftOver
Rhythm software	Laughner, et al.	http://efimovlab.org/content/rhythm
Dataquest software	Data Sciences International	
Origin Pro	OriginLab	
IonWizard	IonOptix	
FlowJo	Tree Star	
Vevolab 2.2.0	Fujifilm Visualsonics	